Collective β-lactam resistance in *Escherichia coli* due to β-lactamase release upon cell death

Rotem Gross[1,*], Muhittin Mungan[1,*], Suman G. Das[2,3,1], Melih Yüksel[1], Berenike Maier[1], Tobias Bollenbach[1], Joachim Krug[1,†], and J. Arjan G.M. de Visser[3,†]

[1]Institute for Biological Physics, University of Cologne, Cologne, Germany
[2]Institute of Ecology and Evolution, University of Bern, Bern, Switzerland
[3]Swiss Institute of Bioinformatics, 1015 Lausanne, Switzerland
[4]Laboratory of Genetics, Wageningen University & Research, Wageningen, The Netherlands
* Equal contribution
† Corresponding authors

October 14, 2024

Abstract

Collective antibiotic resistance occurs when populations of bacteria survive antibiotic treatments that are lethal to individual bacteria, which affects the efficacy of drug therapies. Several mechanisms may lead to collective resistance, including the production of drug-degrading enzymes. Here, we integrate experiments with mathematical modeling to understand the collective survival of *Escherichia coli* challenged with cefotaxime. We observe complex dynamics, involving initial biomass growth due to filamentation, followed by decline and subsequently growth recovery. We show that production of AmpC, a chromosomal β-lactamase, is responsible for cefotaxime degradation, allowing the resumption of cell division in surviving filaments. Our model suggests that the release of AmpC via cell lysis accelerates antibiotic clearance, and does so particularly in strains with low cell-wall permeability that privatize periplasmic cefotaxime hydrolysis. Our findings support the hypothesis of enhanced survival of β-lactamase-producing bacterial populations via altruistic cell death.

Introduction

The concept of antibiotic resistance extends far beyond the modern clinical use of antibiotics [1]. Resistance genes have been identified in pristine settings, including the Alaskan soil and ocean floor sediments [2, 3], and β-lactamases, key enzymes responsible for resistance against β-lactam antibiotics, are thought to have originated billions of years ago [4, 5]. While the current understanding of the roles of antimicrobials and the associated resistance mechanisms in natural ecosystems is limited, their wide distribution and ancient origins indicate that they may have evolved initially as a defense against resource competitors and predators [6].

In the clinical context, β-lactam antibiotics are the most widely prescribed class of antimicrobial compounds used to treat a variety of infectious diseases [7]. Correspondingly, β-lactam resistance through degradation by β-lactamases has been a major medical concern for decades [4, 8, 9]. The enzymatic breakdown occurs in the periplasm of gram-negative bacteria, but it can also take place extracellularly if the enzyme is excreted or released from lysing cells [10]. Both modes of degradation reduce the extracellular concentration of the drug, which makes β-lactamase production a paradigm of a public good that benefits producing as well as non-producing cells [11, 12, 13, 14]. β-lactamases and other antibiotic-modifying enzymes thus make antibiotic resistance a collective property of the bacterial population [15, 16]. A common manifestation of collective resistance is the inoculum effect, where the minimal inhibitory drug concentration (MIC) increases with cell density [12, 14, 15, 17, 18].

Previous work on the social effects of β-lactamase production has mostly considered communities of producing and non-producing strains [10, 11, 13, 19, 20]. Studies of collective β-lactamase-induced resistance of isogenic populations have been limited to global inferences during the establishment of colonies from single cells [17, 21, 22] or the survival of populations of varying size [18].

Here, we combine experiments and modeling to analyse the contribution of β-lactamase production and release through cell death to the survival of isogenic populations of *Escherichia coli* in liquid culture in the presence of cefotaxime, a third generation cephalosporin. Bacterial populations exposed to β-lactam antibiotics at near-lethal concentrations frequently display a complex initial response, where a transient increase in biomass is followed by a decline and a subsequent recovery. While this pattern has been reported in numerous experimental studies dating back at least 50 years [23, 24, 25, 26, 19], the underlying mechanisms have remained obscure.

We will demonstrate that, in our experiments, these complex growth dynamics arise from an interplay of transient tolerance due to the formation of filamentous cells and breakdown of the antibiotic by AmpC, a chromosomally encoded β-lactamase [27] known to be involved in adaptation to β-lactams [28]. Filamentation is a common morphological response to β-lactam antibiotics [29, 30], which reflects the mode of action of these drugs. β-lactams interfere with the synthesis of bacterial cell walls, which is achieved through binding to specific proteins called penicillin-binding proteins (PBPs). Cefotaxime interferes primarily with PBP3, which plays a central role in the divisome, the protein complex involved in cell division. Inhibition of PBP3 obstructs cell division and leads to the formation of filamentous bacterial cells [31, 32, 33, 34, 19, 20]. A key element of our investigation is a kinetic model of the intra- and extracellular enzymatic breakdown of cefotaxime, which we couple to the production and decay of biomass obtained from experimental growth curves. Based on this model, we will show that the contribution of cell lysis to collective survival depends on the level of AmpC privatization, suggesting that cell death may be altruistic [16, 35].

Results

Growth of *E. coli* in the presence of cefotaxime (CTX) shows complex dynamics associated with filamentation, death and recovery

Growth curves of *E. coli* strain REL606 in the presence of increasing CTX concentrations show qualitative differences (Figure 1A). For low CTX concentrations, biomass increases monotonically, saturating at large times. For concentrations between $0.042\,\mu$g/ml and $0.262\,\mu$g/ml, the curves exhibit non-monotonic behavior: the initial growth phase is followed by a decay of biomass until around 15h, before a recovery phase with the resumption of growth sets in. Finally, at even higher concentrations the initial growth is followed by a monotonic decay of biomass, and the populations do not consistently recover. Figure 1B summarizes the growth, decay and recovery rates in these three phases as a function of initial CTX concentration (see the SI for details).

To elucidate the origins of these complex growth dynamics, we first analyzed samples from different time points of populations growing at 0.08 μg CTX/ml under the microscope (Figs. 1C and D). Until biomass peak P, cells become increasingly elongated into filaments. Between time points P and Q, when the biomass is decaying, the number of elongated cells decreases in consecutive images. Around $t = 14$h (point Q in panel C), the recovery phase sets in. Already at this time, normal-size cells are visible, which by $t = 17.5$h have taken over the whole population.

The close similarity of the replicate growth curves measured at the same CTX concentration in Figs. 1A and C makes it unlikely that spontaneous mutations cause the recovery of growth at intermediate CTX concentrations. Regrowth experiments with 80 replicate cultures essentially rule out this possibility (see Fig. S1), which was confirmed by whole genome sequencing (see Materials and Methods).

Growth recovery can be explained by filaments resuming cell division when CTX is removed

We hypothesize that the resumption of cell division during recovery is due to the reduction of CTX in the medium. To see whether normal size cells survive CTX stress or filamentous cells resume cell division, we observed cell growth in a microfluidic chamber. We first treated the bacterial population with a standard LB medium containing $0.2\,\mu$g CTX/ml (causing non-monotonic growth) for 2.5 h, followed by the same growth medium without CTX for 20 h (Fig. 2A). By observing one or a few cells per field of view over time, we were able to follow their response to the removal of CTX. As expected, we found that during the initial flow with CTX, the cells formed filaments (Fig. 2B). About 50 minutes after the end of the treatment with CTX, we observed that filamented cells started to divide again (see Fig. 2C and Supplemental Movie). We, therefore, conclude that the transition from growth decay to growth recovery in Fig. 1A is due to the onset of division of

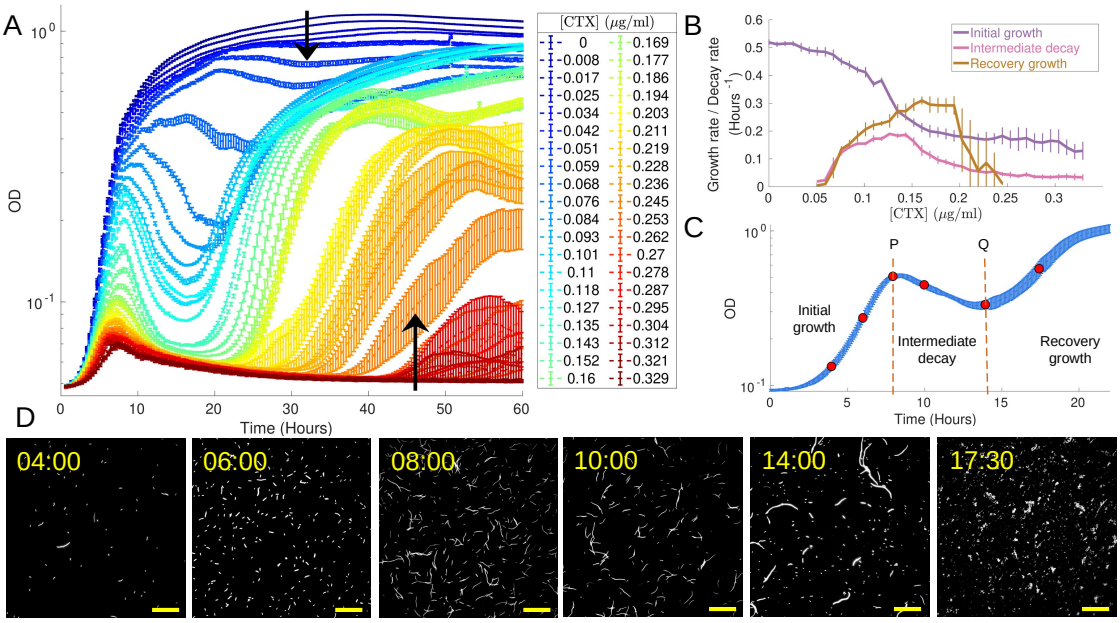

Figure 1: **Non-monotonic growth dynamics of *E. coli* REL606 in the presence of cefotaxime (CTX). A**: Growth curves (measured as optical density, OD, at 600nm) in the presence of varying concentrations of CTX. Each curve shows the average and standard deviation (SD) of OD of 24 replicate cultures initiated with $5 \cdot 10^5$ cells/ml. Non-monotonic growth, involving initial growth, decay and recovery, is observed at CTX concentrations between 0.042-0.262 μg/ml (range boundaries are indicated by black arrows). Beyond a CTX concentration of 0.262 μg/ml, large fluctuations between replicate cultures occur and are accompanied by recovery times exceeding 40h. **B**: Estimates of the average and SD of the maximum growth, decay and recovery rate, attained in the three regimes of the OD growth curves shown in panel A, as a function of CTX concentration (see SI and Fig. S7 for details on the feature extraction). **C**: Mean and SD growth curves of 16 replicate cultures grown at 0.08 μg CTX/ml. The vertical dashed lines mark the initial OD peak P and minimum Q, separating the three growth phases – growth, decay, and recovery. **D**: Microscope images sampled from the time points marked in red in panel C, showing increasing numbers of filamentous cells during initial growth and dominance of normal-size cells during recovery. The yellow length bar corresponds to 100 μm.

filamented cells. In agreement with Ref. [36], we observe that the resumption of cell division of the filaments can occur along any septum and there is no preference for budding off normal-sized cells from the tips of filaments.

Spent medium from CTX-treated cultures accelerates growth resumption

The microfluidic chamber experiment suggests that growth recovery in the batch culture experiments (Fig. 1) is due to the removal of CTX by the growing cells. To determine the remaining amount of CTX at the onset of the recovery phase in the batch cultures, we designed three spent medium experiments (see Materials and Methods). In each experiment, we grow *E. coli* REL606 for 14 h in LB medium at a reference concentration of 0.08 μg CTX/ml, which corresponds to the lower range of concentrations for which we see filamentation and complex growth (see Fig. 1C). We then filter out the cells and mix the resulting spent medium with freshly made LB medium consisting of nutrients and a prescribed amount of CTX. The amount of CTX in the added fresh medium was adjusted such that, under the assumption that all CTX has been removed in the spent medium fraction, the CTX concentration in the mixture reaches a prescribed nominal value $[\mathrm{CTX}]_m$. If not all CTX had been removed from the spent medium fraction by the bacteria, the actual concentration in the mixed medium would thus exceed $[\mathrm{CTX}]_m$.

In the first experiment, growth in the absence and presence of 45% of spent medium was compared for four $[\mathrm{CTX}]_m$ (Fig. 3A). Whereas in the absence of CTX, spent medium does not affect growth as expected, the spent medium unexpectedly *enhances* growth in the presence of CTX, indicating protection beyond the complete removal of CTX in the spent medium fraction.

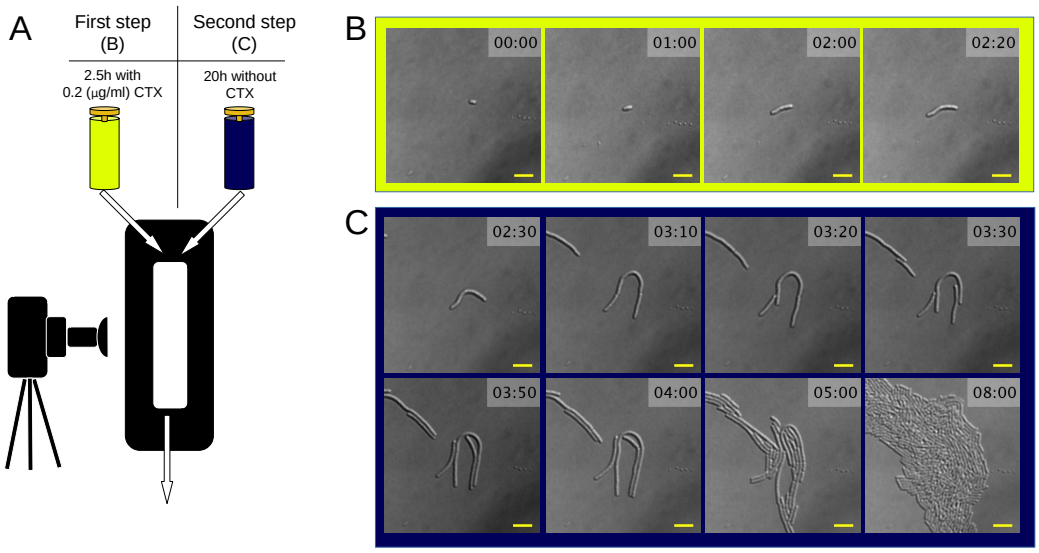

Figure 2: **Filamentous cells resume cell division when CTX is removed. A**: *E. coli* REL606 was grown in a microfluidic flow chamber connected consecutively to two syringes, enabling the supply of nutrient medium with and without CTX. During the first 2.5h, nutrient medium with $0.2\,\mu$g CTX/ml (lemon green) was injected, followed by 20h of CTX-free nutrient medium (dark blue). **B**, **C**: Microscope images from the two phases of the experiment (B: medium with CTX; C: medium without CTX). During exposure to CTX, the cell in the center of view starts to filament. Filamentation continues until 3h10, i.e. 40 min after exposure to CTX was stopped. Cell division accompanied by elongation of filaments occurs between $t = 3$h20 and $t = 4$h, resulting in dividing cells that are still larger than their normal size. However, by $t = 8$h all cells are normal-sized. The yellow length bar corresponds to $10\,\mu$m.

The second experiment was a repetition of the first experiment, but with more variation in the spent medium fraction ϕ, nominal concentrations $[\text{CTX}]_m$, and using sonication during the preparation of the spent medium to maximize the release of protective agent from the cells. The area under the growth curves (AUC) shows a negative impact of spent medium in the absence of CTX, presumably due to nutrient depletion, but for CTX concentrations above the concentration used to produce the spent medium, growth increases systematically with spent medium fraction (Fig. 3B). We also demonstrated the protectiveness of the spent medium on agar medium (S2). In the third experiment, we asked whether the protective effect of spent medium is sensitive to heat, which would suggest it is conferred by a protein. To test this, the spent medium was subjected to a heat treatment prior to the mixing with fresh medium. The growth curves show that heating the spent medium reduces its protection ability in the presence of CTX (Fig. 3C), but has no effect in fresh medium (Fig. 3D), suggesting that a protein secreted by the bacteria is the cause of protection.

AmpC β-lactamase expression accelerates growth recovery in the presence of CTX

Based on the results presented in the preceding section, it appears that the protective effect of the spent medium is related to a protein released by the cells. We will argue that β-lactamase AmpC is a likely candidate, since REL606 does not contain plasmids and AmpC is the only chromosomally-encoded enzyme with β-lactamase activity (https://ecoliwiki.org/colipedia/index.php/Category:Gene_List:REL606).

To test this hypothesis, we performed a parallel set of experiments using the *E. coli* K12 strain, for two reasons. First, the availability of the ASKA [37] and KEIO [38] strain collections for K12 (see Materials and Methods for details) allowed us to vary the expression level of *ampC*, which K12 expresses at a basal level like REL606 [39, 27]. Second, chemical rate constants and other parameters affecting the hydrolysis of CTX by K12's AmpC have been determined [40, 41], which implies that we can link the delay times marking the onset of the recovery phase to the reaction

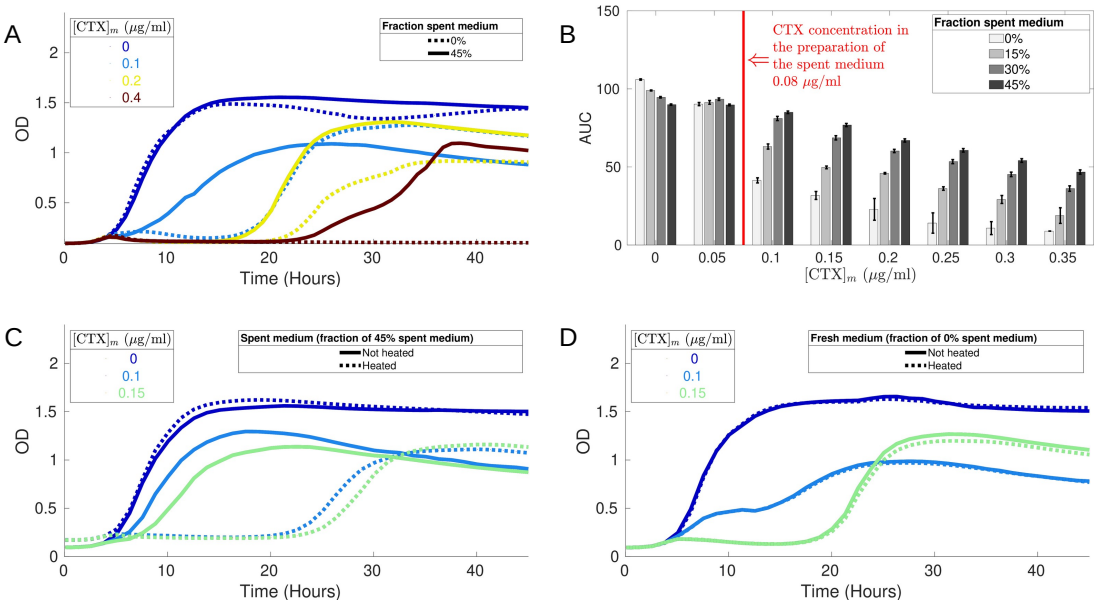

Figure 3: **Spent medium from CTX-treated *E. coli* REL606 cultures is protective. A**: Growth curves at four $[\mathrm{CTX}]_m$ of cultures containing 0 (dashed lines) or 45% (solid lines) spent medium. The spent medium was extracted from overnight cultures grown in the presence of 0.08 μg CTX/ml. $[\mathrm{CTX}]_m$ are nominal initial concentrations in mixed cultures under the assumption that all CTX in the spent medium fraction was removed. **B**: Bacterial growth (measured by the area under the growth curve, AUC, during 30h) at different spent medium fractions ϕ (harvested after 10 s of sonication to lyse the cells) and $[\mathrm{CTX}]_m$. **C**: The protective effect of 45% spent medium in the presence of CTX disappears after heating (98°C for 30 minutes). **D**: Heating has no effect on growth in fresh medium.

kinetics of CTX hydrolysation by quantitative modeling.

Growth behavior of *E. coli* K12 $\Delta lacA$ (Fig. S3) is qualitatively similar to REL606 (Fig. 1A), except that non-monotonic growth sets in at a fivefold lower CTX concentration and the transient decay of biomass is shallower, suggesting lower lysis rates. In order to assess the effect of AmpC expression on growth recovery, we used strain JW4111 from the ASKA collection. This strain contains *ampC* under an inducible promoter on a multicopy plasmid (next to its copy in the chromosome), allowing regulated expression by varying the concentration of inducer IPTG in the medium. We grew JW4111 with three different concentrations of IPTG for 24 h without CTX, filtered out the cells, mixed the remaining spent medium with fresh medium and then let the bacteria grow in the mixed medium in a CTX concentration gradient in the absence of IPTG. Expression of AmpC in the spent medium strongly accelerates growth recovery and causes complete protection for the highest expression level at CTX concentrations far beyond concentrations that are lethal in the absence of spent medium (Fig. 4A).

We then repeated the experiment at intermediate AmpC induction by splitting the spent medium into two fractions. Adding the β-lactamase inhibitor boronic acid to one fraction led to a substantial reduction of growth (Fig. 4B). To confirm the causal role of AmpC in CTX removal and growth recovery, we performed two further experiments. First, we over-expressed each *amp* gene separately, using strains from the ASKA collection and measured the growth on a CTX gradient. The data shown in Fig. S4 clearly demonstrate that only over-expression of AmpC confers increased CTX resistance. Second, we harvested the spent medium from sonicated overnight cultures of the KEIO deletion strains $\Delta ampC$ and $\Delta lacA$, and grew K12 $\Delta lacA$ in mixed media with varying CTX concentrations. At intermediate CTX concentrations, spent medium from the strain $\Delta lacA$, which expresses AmpC, enhances growth relative to that in the spent medium extracted from $\Delta ampC$ (Fig. 4C). Taken together, these findings firmly validate our hypothesis that the observed protection is due to CTX breakdown by AmpC β-lactamase.

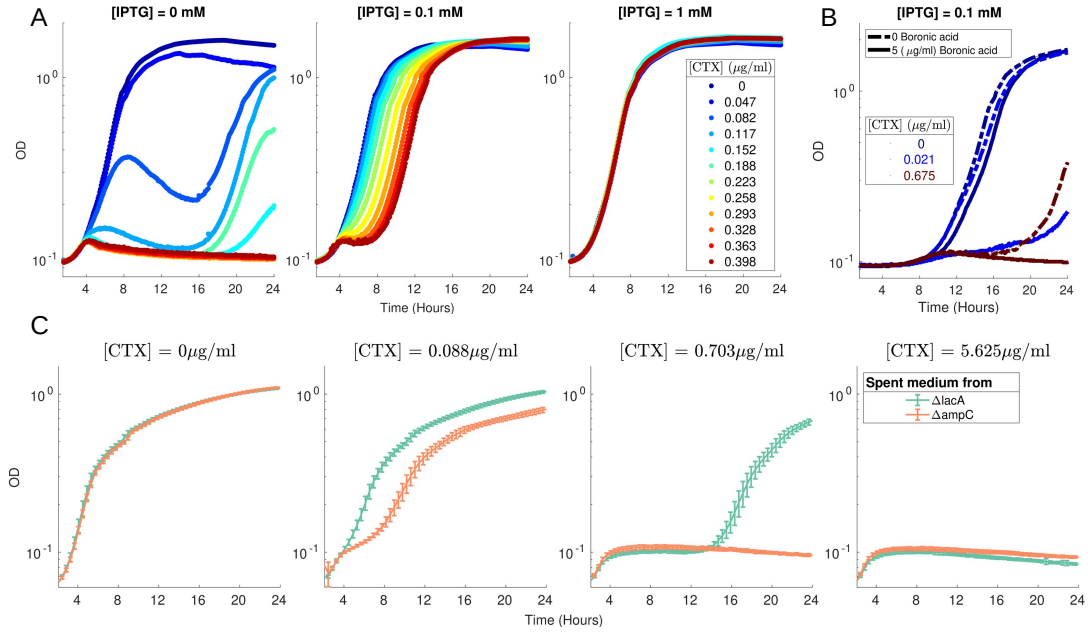

Figure 4: **AmpC expression accelerates growth recovery in CTX. A**: Increased expression of AmpC from a plasmid accelerates growth recovery and allows for monotonic growth at CTX concentrations that fully inhibit growth in the absence of AmpC induction. The three panels show growth curves of *E. coli* JW41111 (ASKA collection, see Materials and methods) in spent media harvested from overnight cultures, grown in the absence of CTX, of the same strain without and with two levels of expression of AmpC induced by IPTG. Note that the growth curves in the leftmost panel display higher OD and a more pronounced non-monotonicity than the corresponding curves for K12 $\Delta lacA$ in Fig. S3. This likely reflects higher AmpC expression due to its higher copy number and leakiness of the inducible promoter. **B**: The addition of boronic acid, which binds to AmpC and inhibits its function, removes the protective effect of AmpC at an intermediate expression level in the presence of CTX. **C**: Growth of K12 $\Delta lacA$ in fresh medium mixed with 45% spent medium from overnight cultures of strains K12 $\Delta lacA$ or $\Delta ampC$ in the absence of CTX, at four different CTX concentrations.

A kinetic model of CTX hydrolysis by AmpC predicts the timing of growth resumption

The scenario emerging from our results is that the observed growth recovery following decay is due to hydrolysis of CTX by AmpC. Consequently, growth resumes once the drug concentration has been reduced below a threshold level. To corroborate this scenario, we developed a model of CTX hydrolysis by AmpC in order to predict recovery times and compare these to observations.

In the model we assume that CTX is hydrolysed by AmpC at two locations: in the periplasm after diffusion of CTX molecules through porins in the outer membrane, and in the extracellular medium after the periplasmic release of AmpC by cell lysis. We use the experimentally obtained growth curves to estimate the amount of non-lysed and lysed biomass at any given time during the experiment, which we then take as input to calculate (i) the amount of AmpC production (by the non-lysed biomass), (ii) the fraction released into the medium upon lysis, and coupled to this, (iii) the total amount of CTX hydrolysed over time. Similar modeling approaches have been used by other groups [12, 18, 34, 42]. Here, we aim for a maximally parsimonious description that explains the observed kinetics using a minimal set of assumptions and parameters. A detailed discussion of the model and its predictions is provided in the SI. In the following, we outline the main ingredients and present our results.

We consider first the hydrolysation of CTX in the periplasm [40, 41, 43]. An equilibrium CTX concentration inside the periplasm is achieved when the diffusion rate of CTX molecules into the periplasm is balanced by the rate of their hydrolysis by AmpC. The CTX concentration difference across the outer membrane is then given by the Zimmermann-Rosselet equation [44],

$$C - C_p = \kappa \frac{C_p}{1 + C_p/K_m}, \tag{1}$$

which relates the extracellular and periplasmic CTX concentrations C and C_p to each other via the dimensionless parameter (see Materials and Methods for details)

$$\kappa = k_{\text{cat}} \frac{E}{K_m} \frac{\mathcal{V}_{\text{peri}}}{PA}. \tag{2}$$

Here, K_m and k_{cat} are the Michaelis-Menten reaction parameters describing CTX hydrolysis, P is the permeability constant of the outer membrane, A is the surface area of *E. coli*, $\mathcal{V}_{\text{peri}}$ is the periplasmic volume and E is the enzyme concentration inside the periplasm. The dimensionless parameter κ is the ratio of the rates of the hydrolysation and influx of CTX in the periplasm. Equation (1) shows that when κ is small, so that the hydrolysation rate is low relative to the influx of CTX, the CTX concentrations outside the cell and within the periplasm are nearly equal. Conversely, when κ is large and the CTX hydrolization rate is larger than its influx, the concentration C_p of CTX inside the periplasm is much lower than outside.

We next estimate the time-dependence of the CTX concentration in the extracellular medium by taking into account the reaction kinetics as well as the growth and lysis of biomass. For *E. coli* K12, Nikaido and collaborators have measured the permeability P, as well as the reaction constants for CTX hydrolysation by the chromosomally encoded β-lactamase AmpC [40, 41]. We therefore consider first the non-monotonic growth of *E. coli* K12 (Fig. S3), which display three regimes: an initial growth phase during which the OD reaches a local maximum at time t_P, an intermediate decay phase, where the OD decreases monotonically up to a time t_Q, and a recovery phase after t_Q during which the OD starts to grow again. We assume that the onset of the recovery phase is determined by the time at which the CTX concentration falls below the value for which the OD growth is still monotonic, i.e. $C = 0.015\,\mu$g/ml for *E. coli* K12 (Fig. S3).

Figure 5A shows a comparison of the empirically observed recovery times $\tau_{\text{obs}} = t_Q - t_P$ for *E. coli* K12, as extracted from the growth curves, with the predicted recovery times τ_{pred} from our model. To obtain the latter, we only varied the number n_β of AmpC molecules per normal-sized cell. Note that the recovery times predicted by our model are comparable with the experimentally measured times. Moreover, for $n_\beta = 700$ AmpC molecules per cell (i.e. in line with previous estimates [45]), we obtain recovery times that follow the data points reasonably well over a broad range of CTX concentrations. In view of the minimal character of our model, which does not include physiological changes in, e.g., the production rate of AmpC or cell wall permeability, the agreement is rather satisfactory.

The contribution of cell lysis to growth recovery depends on the level of AmpC privatization

Based on the estimate $n_\beta = 700$ for the number of AmpC molecules per *E. coli* K12 cell (Fig. 5A), we find that $\kappa_{K12} = 0.39$ (see Materials and Methods). To determine the CTX concentration gradient across the outer membrane from Eq. (1), we use the cross-over from monotonic to non-monotonic growth as an indicator that CTX concentrations within the periplasm have reached levels at which cell growth starts to be affected. As mentioned above, this happens around concentrations of $C = 0.015\,\mu$g CTX/ml (Fig. S3). With the estimated value of κ_{K12}, we find from (1) that the corresponding concentration inside the periplasm is $C_p = 0.011\,\mu$g/ml. We conclude that for *E. coli* K12 at sub-lethal drug concentrations, the transport of the drug across the outer membrane is sufficiently high to maintain similar CTX concentrations inside and outside the cell.

Recall that the magnitude of the CTX concentration gradient across the outer membrane is governed by κ, which in turn determines the collective benefit of cell lysis of β-lactamase-producing cells. To see this, note that the hydrolysis rates are proportional to the product of enzyme and substrate concentrations (see Eq. 5 in the SI). Thus under conditions where AmpC concentrations are higher inside cells and CTX concentrations are higher outside cells, the release of AmpC will generally speed up hydrolysis. The extent of acceleration of CTX hydrolysis via cell lysis will depend on parameter κ. A detailed analysis shows that this effect is borne out under general conditions (see SI): for a given enzyme concentration E, a larger value of κ leads to faster reduction of CTX in the medium when hydrolysis happens outside the cells compared to within the periplasm. Since β-lactamases are released into the extracellular medium predominantly by cell lysis [46], we conclude that for bacterial strains with large κ, cell lysis is expected to speed up CTX hydrolysis, which may be beneficial to the survival of the population as a whole. The parameter κ, therefore, describes the extent to which intra-periplasmic hydrolysis affects the extracellular CTX concentration, and is similar to the privatization parameter introduced in [18].

We will now argue that the AmpC-mediated breakdown of CTX in *E. coli* REL606 occurs in the regime of large κ. While we were not able to find published estimates for P, k_{cat} and K_m for a

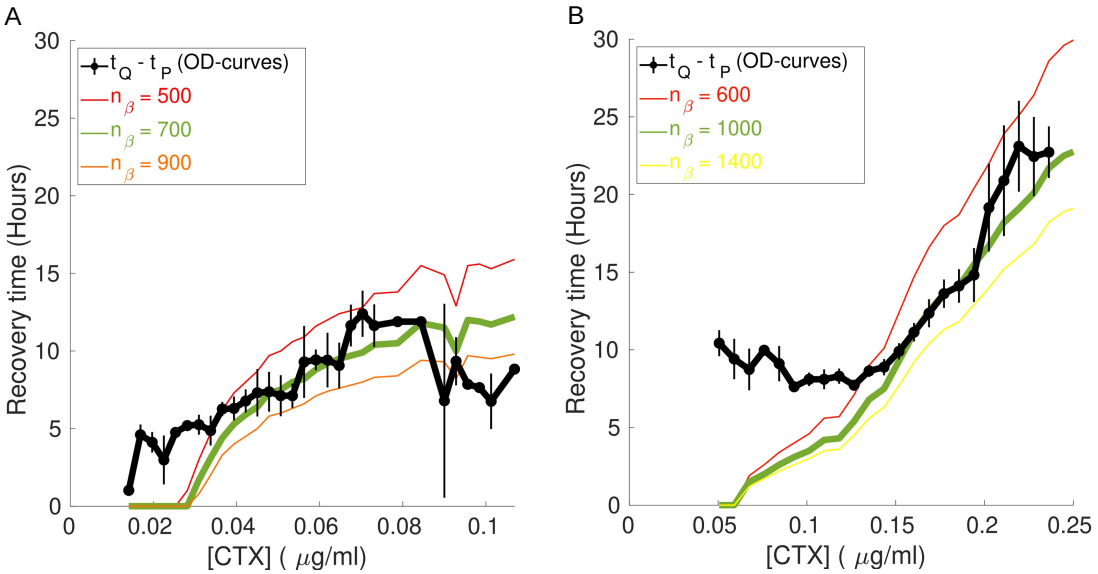

Figure 5: **Model predictions of the time required for AmpC to hydrolyse CTX are consistent with observed recovery times.** **A**: Comparison of recovery times of *E. coli* K12 inferred from the growth curves shown in Fig. S3 (black lines and data points) with predictions from a kinetic model, based on estimates of CTX hydrolysis by lysed and non-lysed cells, using the number n_β of AmpC molecules per normal-sized cells as a free parameter. The best agreement is obtained for $n_\beta = 700$. **B**: The same comparison of predicted and observed recovery times inferred from the growth curves shown in Fig. 1A for *E. coli* REL606, showing reasonable agreement for $n_\beta = 1000$.

direct evaluation of κ, we can obtain an estimate by assuming that the cross-over from monotonic to non-monotonic growth occurs at the same periplasmic CTX concentrations for REL606 as for K12, i.e. $C_p = 0.011\,\mu$g/ml (see above). From Fig. 1, we see that for REL606 the cross-over to non-monotonic growth happens around $C = 0.06\,\mu$g/ml. Assuming that the catalytic capacity of AmpC is comparable for K12 and REL606, and using (1), we can infer from C and C_p that $\kappa_{\text{REL606}} = 5.0$. It is tempting to speculate that the observed higher lysis rate of REL606 relative to K12 (Figs. 1A and S3), is an adaptive response to REL606's larger κ. At any rate, using these parameter values, the recovery times for REL606 can be predicted from the OD curves in Fig. 1A in the same way as for K12 (see SI), showing the best agreement with the empirical data for $n_\beta = 1000$, although for a more limited range of CTX concentrations (Fig. 5B). The inferred 1.4-fold larger value of n_β for REL606 is in agreement with the 1.4-fold greater total per-biomass hydrolysis we measured for REL606 relative to K12 using the chromogenic substrate nitrocefin (see Fig. S5).

Discussion

Understanding bacterial responses to antibiotic treatments is critical for the future efficacy of antibiotic therapies. These responses are often studied at the level of single bacterial cells, whereas responses of individual bacteria are not always predictive for the survival of bacterial populations, which may involve also cooperative interactions [16]. Cooperative interactions leading to collective antibiotic resistance can be caused by diverse mechanisms, including by the production of antibiotic-degrading enzymes, such as β-lactamases [16]. Given the substantial health problems caused by β-lactamase-producing infections [47], it is particularly urgent to better understand the mechanisms and conditions promoting collective β-lactam survival.

Previous studies of population-level responses to β-lactams reported positive density-dependent effects on survival from β-lactamase production [48, 49, 50, 17, 18], the involvement of β-lactam-induced filaments with delayed lysis [33, 34, 19, 51], and complex growth dynamics at near-lethal β-lactam concentrations, involving population growth, death and recovery [23, 24, 25, 26, 19].

In addition, a collective survival benefit was shown for intermediate levels of programmed cell death in an engineered bacterial strain expressing an inducible suicide module and a cytoplasmic β-lactamase [35].

Our present study integrates mathematical modelling and experiments, aimed at understanding the complex growth dynamics we observed when we challenged laboratory *E. coli* strain REL606 with the cephalosporin cefotaxime (Fig. 1A). Our findings advance current insights in multiple ways. First, our results demonstrate the important role for cell death in the release of β-lactamase and collective antibiotic breakdown and survival at near-lethal concentrations of cefotaxime in two laboratory strains of *E. coli* expressing AmpC β-lactamase. Different from previous work with an engineered strain expressing a cytoplasmic β-lactamase that cannot hydrolyse antibiotic without cell death, AmpC is a clinically important β-lactamase, encoded on the chromosomes of many *Enterobacteriaceae* and recently also on transmissible plasmids [39, 52]. Like most β-lactamases, AmpC is functional in the periplasm, hence contributes to environmental CTX degradation via both periplasmic and environmental hydrolysis after cell lysis. Most notably, our results suggest that the contribution of cell death to collective survival depends on the level of privatization of periplasmic AmpC-mediated CTX hydrolysis, i.e. the ratio of periplasmic CTX hydrolysis and CTX flux across the outer-membrane, measured by compound parameter κ (Eq. (2)). Cell death allowing environmental CTX hydrolysis makes a stronger contribution to CTX clearance in bacteria with larger values of κ.

Whether bacteria have evolved programmed altruistic cell death as an adaptive collective β-lactam survival strategy, as suggested by Tanouchi et al. [35], remains to be seen. In this light, it is interesting that we find a higher rate of cell death prior to recovery for *E. coli* strain REL606 with putative lower cell-wall permeability than strain K12. However, it is unclear how cell lysis rates are regulated more generally. To maximize population-level β-lactam survival, one would expect that lysis rates are regulated with respect to AmpC periplasmic hydrolysis capacity (i.e. parameter κ), as well as in response to local cell density and environmental antibiotic concentration. A possible mechanism to regulate cell death in response to cell density is MazEF-mediated cell death, which is regulated via a quorum-sensing pentapeptide [53]. Cell death may also be tuned via the coordination of cell wall synthesis and degradation [54]. AmpC expression is low but inducible via AmpR in response to β-lactams in most Enterobacteriaceae [27]. However, *E. coli* lacks *ampR*, hence AmpC expression is not inducible, but is growth rate-dependent in *E. coli* K12 [39]. Whether and how this contributes to cell lysis and collective β-lactam survival, is presently unknown. A possible route forward suggested by our work, is to determine the role of cell death in the collective β-lactam survival of strains that differ in hydrolysis capacity and membrane permeability, by experimentally varying the compound parameter κ.

A further advance from our study is the observation that the production and release of β-lactamases responsible for collective survival is due to filamentous cells. Filamentation is a known response to β-lactams via two pathways: as downstream response of SOS induction [55], but also by binding of β-lactams like cefotaxime to PBP3, an essential component of the divisome [56, 54]. Filaments have been associated with enhanced β-lactam tolerance through delayed cell division [33, 51]. In addition, lysis rates of filaments have been shown to depend on the activation of cell division [54], as well as on filament length [30, 34], and filaments have been associated with cross-protection against β-lactams [57] via the production of β-lactamases [19]. Filaments have also been suggested to accelerate evolution of antibiotic resistance through enhanced tolerance, mutation and recombination rates [58]. A more quantitative understanding of the physiological properties of filamentous cells seems required to fully understand their role in the evolution of resistance to β-lactams.

Finally, the spent medium assays used in this work to demonstrate the protectiveness of the excreted β-lactamase highlight the broader ecological role of drug-degrading enzymes. In contrast to other resistance mechanisms which benefit only the current population, these enzymes prime the environment in such a way that the regrowth of subsequent populations is facilitated. This effect may be particularly important in fragmented habitats, where the bacteria are cleared in some compartments which are subsequently recolonized [59]. Overall, β-lactamase producing bacteria display a fascinating repertoire of social interactions, which need to be better understood to ensure the continued use of β-lactam antibiotics in combating infectious diseases.

Acknowledgments

We are grateful to the entire Krug group, Bollenbach group, and Maier group for inspiring discussions. We thank Leon Seeger for a thorough reading of the manuscript and valuable comments,

and Gerrit Ansmann for help with statistical analyses. RG would like to thank the Kishony group for their useful comments. MM would like to thank Eric Clément for insightful discussions. This work was funded by DFG SFB 1310 (German Research Foundation, Collaborative Research Centre 1310, project number 325931972).

Contributions

R.G.: Conceptualization (equal); Investigation (lead); Methodology - experiments (lead); Writing – original draft (equal); Visualization (equal).

M.M.: Conceptualization (equal); Modeling and data curation (lead); Formal analysis (lead); Methodology - computational (lead); Writing – original draft (equal); Visualization (equal).

S.G.D.: Conceptualization (supporting); Writing – review (supporting).

M.Y.: Writing – review (supporting); Methodology - microfluidic experiment (supporting) and WGS (lead).

T.B.: Conceptualization (supporting); Writing – review (supporting).

B.M.: Conceptualization (supporting); Writing – review (supporting).

J.K.: Conceptualization (equal); Project administration (equal); Writing – review and editing (lead); Funding acquisition (equal); Supervision (equal); Visualization (equal); Methodology - computational (supporting).

J.A.G.M.d.V: Conceptualization (equal); Project administration (equal); Writing – review and editing (lead); Funding acquisition (equal); Supervision (equal); Visualization (equal); Methodology - experiments (supporting).

References

[1] Vanessa M D'Costa, Christine E King, Lindsay Kalan, Mariya Morar, Wilson WL Sung, Carsten Schwarz, Duane Froese, Grant Zazula, Fabrice Calmels, Regis Debruyne, et al. Antibiotic resistance is ancient. *Nature*, 477(7365):457–461, 2011.

[2] Heather K Allen, Luke A Moe, Jitsupang Rodbumrer, Andra Gaarder, and Jo Handelsman. Functional metagenomics reveals diverse β-lactamases in a remote Alaskan soil. *The ISME Journal*, 3(2):243–251, 2009.

[3] Marta Toth, Clyde Smith, Hilary Frase, Shahriar Mobashery, and Sergei Vakulenko. An antibiotic-resistance enzyme from a deep-sea bacterium. *Journal of the American Chemical Society*, 132(2):816–823, 2010.

[4] Barry G Hall and Miriam Barlow. Evolution of the serine β-lactamases: past, present and future. *Drug Resistance Updates*, 7(2):111–123, 2004.

[5] Valeria A Risso, Jose A Gavira, Diego F Mejia-Carmona, Eric A Gaucher, and Jose M Sanchez-Ruiz. Hyperstability and substrate promiscuity in laboratory resurrections of precambrian β-lactamases. *Journal of the American Chemical Society*, 135(8):2899–2902, 2013.

[6] William P. J. Smith, Benjamin R. Wucher, Carey D. Nadell, and Kevin R. Foster. Bacterial defences: mechanisms, evolution and antimicrobial resistance. *Nature Reviews Microbiology*, 21:519–534, 2023.

[7] Karen Bush and Patricia A Bradford. β-lactams and β-lactamase inhibitors: an overview. *Cold Spring Harbor Perspectives in Medicine*, 6(8), 2016.

[8] K. Bush. Past and present perspectives on β-lactamases. *Antimicrobial Agents and Chemotherapy*, 62:e01076–18, 2018.

[9] Catherine L Tooke, Philip Hinchliffe, Eilis C Bragginton, Charlotte K Colenso, Viivi HA Hirvonen, Yuiko Takebayashi, and James Spencer. β-lactamases and β-lactamase inhibitors in the 21st century. *Journal of Molecular Biology*, 431(18):3472–3500, 2019.

[10] H. Nicoloff and D. I. Andersson. Indirect resistance to several classes of antibiotics in cocultures with resistant bacteria expressing antibiotic-modifying or -degrading enzymes. *Journal of Antimicrobial Chemotherapy*, 71:100–110, 2016.

[11] Eugene A Yurtsev, Hui Xiao Chao, Manoshi S Datta, Tatiana Artemova, and Jeff Gore. Bacterial cheating drives the population dynamics of cooperative antibiotic resistance plasmids. *Molecular Systems Biology*, 9(1):683, 2013.

[12] Tatiana Artemova, Ylaine Gerardin, Carmel Dudley, Nicole M Vega, and Jeff Gore. Isolated cell behavior drives the evolution of antibiotic resistance. *Molecular Systems Biology*, 11(7):822, 2015.

[13] Isabel Frost, William PJ Smith, Sara Mitri, Alvaro San Millan, Yohan Davit, James M Osborne, Joe M Pitt-Francis, R Craig MacLean, and Kevin R Foster. Cooperation, competition and antibiotic resistance in bacterial colonies. *The ISME Journal*, 12(6):1582–1593, 2018.

[14] Michael J Bottery, Jonathan W Pitchford, and Ville-Petri Friman. Ecology and evolution of antimicrobial resistance in bacterial communities. *The ISME Journal*, 15(4):939–948, 2021.

[15] Nicole M. Vega and Jeff Gore. Collective antibiotic resistance: mechanisms and implications. *Current Opinion in Microbiology*, 21:28–34, 2014.

[16] Hannah R. Meredith, Jaydeep K. Srimani, Anna J. Lee, Allison J. Lopatkin, and Lingchong You. Collective antibiotic tolerance: mechanisms, dynamics and intervention. *Nature Chemical Biology*, 11:182–188, 2015.

[17] Manja Saebelfeld, Suman G. Das, Arno Hagenbeek, Joachim Krug, and J. Arjan G. M. de Visser. Stochastic establishment of β-lactam-resistant Escherichia coli mutants reveals conditions for collective resistance. *Proceedings of the Royal Society B*, 289:20212486, 2022.

[18] Lukas Geyrhofer, Philip Ruelens, Andrew D Farr, Diego Pesce, J Arjan GM de Visser, and Naama Brenner. Minimal surviving inoculum in collective antibiotic resistance. *mBio*, 14(2):e02456–22, 2023.

[19] Xinne Zhao, Philip Ruelens, Andrew D. Farr, J. Arjan G. M. de Visser, and Larysa Baraban. Population dynamics of cross-protection against β-lactam antibiotics in droplet microreactors. *Frontiers in Microbiology*, 14:1294790, 2023.

[20] Andrew D. Farr, Diego Pesce, Suman G. Das, Mark P. Zwart, and J. Arjan G. M. de Visser. The fitness of beta-lactamase mutants depends nonlinearly on resistance level at sublethal antibiotic concentrations. *mBio*, 14:e00098–23, 2023.

[21] H. K. Alexander and R. C. MacLean. Stochastic bacterial population dynamics restrict the establishment of antibiotic resistance from single cells. *Proceedings of the National Academy of Sciences*, 117:19455–19464, 2020.

[22] Manja Saebelfeld, Suman G. Das, Jorn Brink, Arno Hagenbeek, Joachim Krug, and J. Arjan G.M. De Visser. Antibiotic breakdown by susceptible bacteria enhances the establishment of β-lactam resistant mutants. *Frontiers in Microbiology*, 12:698970, 2021.

[23] Edward R. Garrett and Chong Min Won. Kinetics and mechanisms of drug action on microorganisms xvii: Bactericidal effects of penicillin, kanamycin, and rifampin with and without organism pretreatment with bacteriostatic chloramphenicol, tetracycline, and novobiocin. *Journal of Pharmaceutical Sciences*, 62:1666–1673, 1973.

[24] Akira Tsuji, Shoichiro Hamano, Tetsuo Asano, Emi Nakashima, Tsukinaka Yamana, and Susumu Mitsuhashi. Microbial kinetics of β-lactam antibiotics against Escherichia coli. *Journal of Pharmaceutical Sciences*, 73:1418–1422, 1984.

[25] Felix Wong, Sean Wilson, Ralf Helbig, Smitha Hegde, Olha Aftenieva, Hai Zheng, Chenli Liu, Teuta Pilizota, Ethan C Garner, Ariel Amir, et al. Understanding beta-lactam-induced lysis at the single-cell level. *Frontiers in Microbiology*, 12:712007, 2021.

[26] Silvia Kollerová, Lionel Jouvet, Julia Smelková, Sara Zunk-Parras, Alexandro Rodrìguez-Rojas, and Ulrich K. Steiner. Phenotypic resistant single-cell characteristics under recurring ampicillin antibiotic exposure in Escherichia coli. *mSystems*, 9:e00256–24., 2024.

[27] George A. Jacoby. AmpC β-lactamases. *Clinical Microbiology Reviews*, 22:161–182, 2009.

[28] Rotem Gross, Idan Yelin, Viktória Lázár, Manoshi Sen Datta, and Roy Kishony. Beta-lactamase dependent and independent evolutionary paths to high-level ampicillin resistance. *Nature Communications*, 15(1):5383, 2024.

[29] A. D. Gardner. Morphological effects of penicillin on bacteria. *Nature*, 146:837–838, 1940.

[30] George N. Rolinson. Effect of β-lactam antibiotics on bacterial cell growth rate. *Journal of General Microbiology*, 120:317–323, 1980.

[31] J. Buijs, A.S.M. Dofferhoff, J.W. Mouton, J.H.T. Wagenvoort, and J.W.M. Van Der Meer. Concentration-dependency of β-lactam-induced filament formation in gram-negative bacteria. *Clinical Microbiology and Infection*, 14(4):344–349, 2008.

[32] Thea SB Kjeldsen, Morten OA Sommer, and John E Olsen. Extended spectrum β-lactamase-producing Escherichia coli forms filaments as an initial response to cefotaxime treatment. *BMC Microbiology*, 15:1–6, 2015.

[33] Taiyeb Zahir, Dorien Wilmaerts, Sabine Franke, Bram Weytjens, Rafael Camacho, Kathleen Marchal, Johan Hofkens, Maarten Fauvart, and Jan Michiels. Image-based dynamic phenotyping reveals genetic determinants of filamentation-mediated β-lactam tolerance. *Frontiers in Microbiology*, 11:374, 2020.

[34] Kyeri Kim, Teng Wang, Helena R Ma, Emrah Şimşek, Boyan Li, Virgile Andreani, and Lingchong You. Mapping single-cell responses to population-level dynamics during antibiotic treatment. *Molecular Systems Biology*, 19(7):e11475, 2023.

[35] Yu Tanouchi, Anand Pai, Nicolas E. Buchler, and Lingchong You. Programming stress-induced altruistic death in engineered bacteria. *Molecular Systems Biology*, 8:626, 2012.

[36] Martijn Wehrens, Dmitry Ershov, Rutger Rozendaal, Noreen Walker, Daniel Schultz, Roy Kishony, Petra Anne Levin, and Sander J. Tans. Size laws and division ring dynamics in filamentous Escherichia coli cells. *Current Biology*, 28(6):972–979.e5, 2018.

[37] M. Kitagawa et al. Complete set of orf clones of Escherichia coli ASKA library (a complete set of E. coli K-12 ORF archive): Unique resources for biological research. *DNA Research*, 12:291–299, 2005.

[38] T. Baba et al. Construction of Escherichia coli K-12 in-frame, single-gene knockout mutants: the Keio collection. *Molecular Systems Biology*, 2:2006.0008, 2005.

[39] Bengtåke Jaurin, Thomas Grundström, Thomas Edlund, and Staffan Normark. The E. coli β-lactamase attenuator mediates growth rate-dependent regulation. *Nature*, 290(5803):221–225, 1981.

[40] Hiroshi Nikaido. Role of permeability barriers in resistance to β-lactam antibiotics. *Pharmacology & Therapeutics*, 27(2):197–231, 1985.

[41] H Nikaido and S Normark. Sensitivity of Escherichia coli to various β-lactams is determined by the interplay of outer membrane permeability and degradation by periplasmic β-lactamases: a quantitative predictive treatment. *Molecular Microbiology*, 1(3):29–36, 1987.

[42] Virgile Andreani. *Modelling and efficient characterization of enzyme-mediated response to antibiotic treatments*. PhD thesis, Ecole polytechnique, 2020.

[43] H Nikaido, EY Rosenberg, and J Foulds. Porin channels in Escherichia coli: studies with beta-lactams in intact cells. *Journal of Bacteriology*, 153(1):232–240, 1983.

[44] Willy Zimmermann and Armel Rosselet. Function of the outer membrane of Escherichia coli as a permeability barrier to beta-lactam antibiotics. *Antimicrobial Agents and Chemotherapy*, 12(3):368–372, 1977.

[45] Derek N Macklin, Travis A Ahn-Horst, Heejo Choi, Nicholas A Ruggero, Javier Carrera, John C Mason, Gwanggyu Sun, Eran Agmon, Mialy M DeFelice, Inbal Maayan, et al. Simultaneous cross-evaluation of heterogeneous E. coli datasets via mechanistic simulation. *Science*, 369(6502):eaav3751, 2020.

[46] Nikol Kaderabkova, Manasa Bharathwaj, R. Christopher D. Furniss, Diego Gonzalez, Tracy Palmer, and Despoina A.I. Mavridou. The biogenesis of β-lactamase enzymes. *Microbiology*, 168(8), 2022.

[47] Alessandro Cassini, Liselotte Diaz Högberg, Diamantis Plachouras, Annalisa Quattrocchi, Ana Hoxha, Gunnar Skov Simonsen, Mélanie Colomb-Cotinat, Mirjam E Kretzschmar, Brecht Devleesschauwer, Michele Cecchini, et al. Attributable deaths and disability-adjusted life-years caused by infections with antibiotic-resistant bacteria in the EU and the European Economic Area in 2015: a population-level modelling analysis. *The Lancet Infectious Diseases*, 19(1):56–66, 2019.

[48] Itzhak Brook. Inoculum effect. *Reviews of Infectious Diseases*, 11(3):361–368, 1989.

[49] Klas I Udekwu, Nicholas Parrish, Peter Ankomah, Fernando Baquero, and Bruce R Levin. Functional relationship between bacterial cell density and the efficacy of antibiotics. *Journal of Antimicrobial Chemotherapy*, 63(4):745–757, 2009.

[50] Cheemeng Tan, Robert Phillip Smith, Jaydeep K Srimani, Katherine A Riccione, Sameer Prasada, Meta Kuehn, and Lingchong You. The inoculum effect and band-pass bacterial response to periodic antibiotic treatment. *Molecular Systems Biology*, 8(1):617, 2012.

[51] Christine Miller, Line Elnif Thomsen, Carina Gaggero, Ronen Mosseri, Hanne Ingmer, and Stanley N. Cohen. SOS response induction by β-lactams and bacterial defense against antibiotic lethality. *Science*, 305:1629–1631, 2004.

[52] Gian Maria Rossolini, Fabio Arena, Patrizia Pecile, and Simona Pollini. Update on the antibiotic resistance crisis. *Current Opinion in Pharmacology*, 18:56–60, 2014.

[53] Ilana Kolodkin-Gal, Ronen Hazan, Ariel Gaathon, Shmuel Carmeli, and Hanna Engelberg-Kulka. A linear pentapeptide is a quorum-sensing factor required for mazEF-mediated cell death in Escherichia coli. *Science*, 318(5850):652–655, 2007.

[54] Hak Suk Chung, Zhizhong Yao, Nathan W. Goehring, Roy Kishony, Jon Beckwith, and Daniel Kahne. Rapid β-lactam-induced lysis requires successful assembly of the cell division machinery. *Proceedings of the National Academy of Sciences*, 106:21872–21877, 2009.

[55] Amit Mukherjee, Chune Cao, and Joe Lutkenhaus. Inhibition of FtsZ polymerization by SulA, an inhibitor of septation in Escherichia coli. *Proceedings of the National Academy of Sciences*, 95(6):2885–2890, 1998.

[56] Nigel AC Curtis, Rosemary L Eisenstadt, Kath A Turner, and Anthony J White. Inhibition of penicillin-binding protein 3 of Escherichia coli K-12. Effects upon growth, viability and outer membrane barrier function. *Journal of Antimicrobial Chemotherapy*, 16(3):287–296, 1985.

[57] Bing Li, Yong Qiu, Andrew Glidle, Jon Cooper, Han Chang Shi, and Hua Bing Yin. Single cell growth rate and morphological dynamics revealing an "opportunistic" persistence. *Analyst*, 139:3305–3313, 2014.

[58] Julia Bos, Qiucen Zhang, Saurabh Vyawahare, Elizabeth Rogers, Susan M Rosenberg, and Robert H Austin. Emergence of antibiotic resistance from multinucleated bacterial filaments. *Proceedings of the National Academy of Sciences*, 112(1):178–183, 2015.

[59] Nia Verdon, Ofelia Popescu, Simon Titmuss, and Rosalind J. Allen. Habitat fragmentation enhances microbial collective defence. *bioRxiv*, 2024.

[60] Isabel Rathmann, Mona Förster, Melih Yüksel, Lucas Horst, Gabriela Petrungaro, Tobias Bollenbach, and Berenike Maier. Distribution of fitness effects of cross-species transformation reveals potential for fast adaptive evolution. *The ISME Journal*, 17(1):130–139, 2023.

[61] Jeffrey J Power, Fernanda Pinheiro, Simone Pompei, Viera Kovacova, Melih Yüksel, Isabel Rathmann, Mona Förster, Michael Lässig, and Berenike Maier. Adaptive evolution of hybrid bacteria by horizontal gene transfer. *Proceedings of the national Academy of Sciences*, 118(10):e2007873118, 2021.

[62] Haeyoung Jeong, Valérie Barbe, Choong Hoon Lee, David Vallenet, Dong Su Yu, Sang-Haeng Choi, Arnaud Couloux, Seung-Won Lee, Sung Ho Yoon, Laurence Cattolico, et al. Genome sequences of escherichia coli b strains rel606 and bl21 (de3). *Journal of molecular biology*, 394(4):644–652, 2009.

[63] Heng Li and Richard Durbin. Fast and accurate short read alignment with burrows–wheeler transform. *bioinformatics*, 25(14):1754–1760, 2009.

[64] Petr Danecek, James K Bonfield, Jennifer Liddle, John Marshall, Valeriu Ohan, Martin O Pollard, Andrew Whitwham, Thomas Keane, Shane A McCarthy, Robert M Davies, et al. Twelve years of samtools and bcftools. *Gigascience*, 10(2):giab008, 2021.

[65] Melih Yüksel, Jeffrey J Power, Jan Ribbe, Thorsten Volkmann, and Berenike Maier. Fitness trade-offs in competence differentiation of Bacillus subtilis. *Frontiers in Microbiology*, 7:888, 2016.

[66] Xian-Zhi Li, Patrick Plésiat, and Hiroshi Nikaido. The challenge of efflux-mediated antibiotic resistance in gram-negative bacteria. *Clinical Microbiology Reviews*, 28(2):337–418, 2015.

[67] Jigneshkumar Dahyabhai Prajapati, Ulrich Kleinekathöfer, and Mathias Winterhalter. How to enter a bacterium: Bacterial porins and the permeation of antibiotics. *Chemical Reviews*, 121(9):5158–5192, 2021.

[68] J.B. Stock, B. Rauch, and S. Roseman. Periplasmic space in Salmonella typhimurium and Escherichia coli. *Journal of Biological Chemistry*, 252(21):7850–7861, 1977.

Materials and methods

Strains and media

The following ancestral strains were used in this study:

- *E. coli* REL606 knockout strain $\Delta pcnB$.
- *E. coli* K12 $\Delta lacA$ strain JW0333 and $\Delta ampC$ strain JW4111 from the Keio collection [38].
- *E. coli* K12 strains from the ASKA collection that contain specific *amp*-genes on an IPTG inducible high copy number plasmid [37]. The inducible expression from the plasmid occurs in addition to the chromosomal expression, which is likely to lead to strong overexpression. The specific strains used were JW4111 (*ampC*), JW0106 (*ampD*), JW0107 (*ampE*), JW0423 (*ampG*) and JW5052 (*ampH*).

The two K12 strain groups encode resistance genes to chloramphenicol (ASKA) and kanamycin (Keio) that help to prevent contamination. The growth medium used in this study was Sigma-Aldrich LB (Lennox, L3022). Cefotaxime (Sigma-Aldrich, 219504) solutions were freshly prepared (see Supplementary Table 1 for concentrations used).

Growth of *E. coli* strains REL606 and K12 in a linear CTX gradient

We inoculated 24 replicates cultures (inoculum size of $5 \cdot 10^5$ cells per ml) in LB with a linear CTX concentration gradient of 40 CTX concentrations, ranging between $0.0 - 0.329\,\mu$g/ml for Fig 1 and $0.0 - 0.113\,\mu$g/ml for Fig S3. Each set of plates was arranged such that each plate contained four CTX concentrations from the gradient (two rows per concentration), leading to ten plates in total for the 24 replicates. Next, the 10 plates were loaded into a robot system (Liconic incubator at Prime robot) and optical density (OD) at 600 nm was measured approximately every 20 minutes over 60h in the case of Fig 1 and 24h in the case of Fig S3.

Whole genome sequencing after recovery

To check for possible mutations causing the recovery of growth, genomic DNA was isolated from cell suspensions grown overnight at 0 and 0.08 μg CTX/ml, using the NEB Monarch Genomic DNA Purification Kit (Ipswich, USA) according to the manufacturer's instructions. A small aliquot of the isolated DNA was run on a 0.7% agarose gel with a 1 kb plus DNA Ladder (Thermo Scientific) to check for degradation. Non-degraded samples were sent to the Cologne Center for Genomics (Cologne, Germany) for NGS. Sequencing was performed on an Illumina Novaseq 6000 system with 150 bp paired-end reads and an average depth of 600X. Sequence analysis was performed using the pipeline described in [60, 61]. In short, the sequencing reads of the samples were mapped to the genome sequence of REL606 (NCBI Genbank RefSeq NC_012967.1, [62] using Burrows-Wheeler Aligner (v.0.7.17) [63]. Mapped reads were sorted with the sort function of samtools (samtools 1.8) and variants were called with the mpileup function and the call function from bcftools (bcftools 1.8) [64]. To identify deletions and duplications, genome coverage per base was calculated. After smoothing, the coverage with a sliding window of 30 bp, all segments in which the coverage dropped to zero for at least ten bases in a row were defined to be deletions. To be accepted as duplication, the coverage has to hit twice the genome-wide average coverage for ten subsequent bases. While we detected several mutations in both samples relative to the published genome of REL606, no mutations of any type were detected that distinguished the overnight cultures grown at 0 or 0.08 μg CTX/ml, thereby ruling out mutations as cause for growth recovery.

Cell growth in the microfluidic chamber

To track the growth behavior of individual bacteria over time, we used a microfluidic chamber. The flow chamber was made from polyoxymethylene with a cut for the main channel of size $6 \times 56 \times 1$ mm with a hole in the center of size of 6×26 mm and two small holes at each side of the edge. The main channel was filled by polydimethylsiloxane (PDMS), forming a layer with a layout of $0.5\,\mu$m high pillars and a 2 mm gap between each one of them. The two tubes with smaller holes allow media to flow through the chamber (further details of the chamber are given in [65]). To be able to track single cells over time, $\sim 1,000$ cells were inoculated between a glass cover slide and a 1.5 mm-thick agar pad made of Milli-Q Water with 1% Bacto agar (BD). This was integrated into the flow chamber and sealed by picodent twinsil (Picodent) to restrict the flow of

the media between the agar pad and the PDMS, and to prevent leaks. After the flow chamber was sealed, it was placed on the stage of a 30°C heat-controlled inverted microscope (Nikon Eclipse TE2000-E) using a 100X objective. Once the field of view for the imaging was chosen, Differential Interference Contrast (DIC) images were taken every 10 minutes. Two syringes containing media were connected consecutively to the fluidic chamber and controlled by a syringe pump.

The experiment was done in two steps: first, only the syringe with medium containing nutrients and $0.2\,\mu$g CTX/ml was opened at a flow rate of $60\,\mu$l/minute for 2.5h. In the second step, only the syringe with CTX-free nutrient medium was opened at a flow rate of $15\,\mu$l/minute for 20h.

Spent medium experiments

To investigate the antibiotic degradation by the cells, we performed three spent medium experiments. In the first experiment, we aimed to determine whether protection was due to CTX degradation in the spent medium or goes beyond that. In the second experiment, we quantified the level of protection offered by the spent medium. In the third experiment, we tested whether protection was due to a protein and sensitive to heating. For all three experiments, we prepared culture media by mixing the spent medium with different amounts of CTX and fresh nutrients.

To generate the spent medium, we grew *E. coli* in LB containing $0.08\,\mu$g CTX/ml, which induces non-monotonic growth behaviour. The incubation time was 14h, corresponding to the time point at which recovery occurs. After incubation, we filtered out the cells to obtain the spent medium. In the second experiment, we additionally sonicated the medium for 10 seconds before filtration to remove effects from variation in cell lysis during preparation.

In order to obtain a mixed culture medium with a total volume of $V = 200\,\mu$l, we mixed three different media:

- A bacterial culture with a culture volume $V_b = 20\,\mu$l: freshly made LB without CTX was prepared with a cell density of $5 \cdot 10^6$ cells per ml. In the total culture volume V this gives a final inoculum size of $5 \cdot 10^5$ cells per ml.

- Diluted spent medium with a culture volume $V_s = 90\,\mu$l: The harvested spent medium was mixed in different proportions with freshly made LB without CTX. The fractions of the spent medium in this volume were chosen to be $\lambda = 0, \frac{1}{3}, \frac{2}{3}, 1$, leading to the spent medium fractions $\phi = \frac{\lambda V_s}{V} = 0.45\lambda = 0, 0.15, 0.30, 0.45$ in the total culture volume V.

- Fresh medium with [CTX] in a culture volume $V_f = 90\mu$l: Freshly made LB was prepared with a linear CTX gradient. The CTX concentrations $\tilde{c}$ in this volume were chosen in such a way that, under the assumption that no CTX was left in the spent medium, the CTX concentration in the total culture volume V would amount to the prescribed nominal concentration $[\text{CTX}]_m$. This implies that $[\text{CTX}]_m = \frac{\tilde{c}V_f}{V} = 0.45\ \tilde{c}$, which determines $\tilde{c}$ for a given nominal concentration.

The spent medium fractions and CTX concentration used in the different experiments were chosen as follows:

- Experiment 1: Bacterial cultures with spent medium fractions of $\phi = 0\%$ and 45% and fresh medium containing CTX at concentrations $\tilde{c}$ ranging from 0 to 1.222 μg/ml in steps of 0.111 μg/ml, leading to nominal concentrations from 0 to 0.55 μg/ml in steps of $0.05\,\mu$g/ml.

- Experiment 2: Bacterial cultures with spent medium fractions of $\phi = 0\%, 15\%, 30\%, 45\%$ and fresh medium containing CTX at concentrations of $\tilde{c}$ ranging from 0 to 0.777 μg/ml in steps of 0.111 μg/ml, leading to nominal concentrations from 0 to 0.35 μg/ml in steps of $0.05\,\mu$g/ml.

- Experiment 3: Bacterial cultures with spent medium fractions of $\phi = 0\%$ and 45%. For both fractions, the medium was split into two portions, one of which was heated to 98°C for 30 minutes. Subsequently, the heated and non-heated media were mixed with fresh medium containing CTX at concentrations of $\tilde{c}$ ranging from 0 to 0.777 μg CTX/ml in steps of 0.111 μg CTX/ml, leading to nominal concentrations ranging from 0 to 0.35 μg CTX/ml in steps of $0.05\,\mu$g CTX/ml.

After the preparation of the culture medium for each experiment, we measured the OD growth curves using a plate reader.

Protection ability of spent medium in a structured environment

We poured six plates with 20 ml 2% LB + 1.5% agar and 0.25 μg CTX/ml. After the agar in the plates solidified, we placed a drop of 200 μl of spent medium (harvested after 14 h of growth in LB with 0.08 μg CTX/ml) on three different plates, and a drop of 200 μl of fresh LB without CTX on the three other plates (marked by red circles in Fig. S2). Then we let the drops be soaked into the medium for 6h. After the plates were dry, we inoculated a drop of 100 μl of *E. coli* ($5 \cdot 10^5$ cells) and distributed them all over the plate with bacterial cell spreaders. Finally, we incubated the plates overnight at 30°C degrees and subsequently imaged the plates.

Protection ability of spent medium from ASKA and Keio strains

E. coli JW4111 was grown with inoculum size of $5 \cdot 10^5$ cells/ml in three different concentrations of IPTG (0, 0.1 and 1 mM) for 24 h without CTX, cells were filtered out, and the resulting spent medium was mixed with fresh medium (to a final spent medium fraction of 45%) containing a different amount of CTX (see Exp. 7 in Table S1) and OD of the cultures was measured over time.

We repeated the experiment at intermediate AmpC induction, growing *E. coli* JW4111 with inoculum size of $5 \cdot 10^5$ cells/ml with 0.1 mM IPTG overnight and harvesting the spent medium. The spent medium was then split into two fractions and 5μg/ml of boronic acid (a β-lactamase inhibitor) was added to one fraction.

We performed two further experiments. First, we over-expressed (by using 1 mM IPTG) all *amp* genes separately using strains from the ASKA collection (JW4111 (*ampC*), JW0106 (*ampD*), JW0107 (*ampE*), JW0423 *ampG*) and JW5052 (*ampH*)) and measured their growth in varying CTX concentrations (See Exp. 14 in Table S1). Second, we grew ΔampC and ΔlacA strains from the KEIO deletion library overnight in LB broth without CTX. Then both cultures were subjected to sonication separately for 2 minutes to lyse all cells, and the spent media were harvested. Each harvested medium was mixed with fresh medium (to a final spent medium fraction of 45%) with a CTX gradient (See Exp. 9 in Table S1). The OD growth of *E. coli* K12 ΔlacA in each of the mixed media was then measured.

Theoretical description of CTX transport and hydrolysis in the periplasm

The entry of β-lactams into the periplasm occurs through porins and their diffusion across the outer membrane bilayer is negligible [66, 66, 67]. The influx of CTX via porins into the periplasm is assumed to be governed by Fick's law

$$\mathcal{V}_{\text{peri}} \frac{\mathrm{d}C_p}{\mathrm{d}t} = PA(C - C_p),$$

where P is the permeability constant, A is the *E. coli* surface area, $\mathcal{V}_{\text{peri}}$ is the periplasmic volume, and C and C_p are the CTX concentration outside the cell and inside the periplasm, respectively. The hydrolysis of CTX via β-lactamases in the periplasm follows a Michaelis-Menten type kinetics

$$\frac{\mathrm{d}C_p}{\mathrm{d}t} = -k_{\text{cat}} E \frac{C_p}{K_m + C_p},$$

where E is the concentration of β-lactamase, while k_{cat} and K_m are the rate constants of the CTX hydrolysis reaction kinetics.

Equilibrium is established once the concentration of CTX inside the periplasm is constant in time, implying that the influx rate of CTX via porins is balanced by the hydrolysis rate inside the periplasm. This leads to the Zimmermann-Rosselet equation [44], Eqs. (1) and (2) of the main text:

$$C - C_p = \kappa \frac{C_p}{1 + C_p/K_m}, \quad \text{with} \quad \kappa = k_{\text{cat}} \frac{E}{K_m} \frac{\mathcal{V}_{\text{peri}}}{PA}. \tag{3}$$

Note that for typical values of CTX concentrations the equilibrium drug concentration inside the periplasm is established within seconds [40], i.e. much faster than the time scale of hours over which the biomass changes in our experiments.

The dimensionless parameter κ is the ratio of the rates of the hydrolysation and influx of CTX in the periplasm. It summarizes several cell-specific properties, such as its outer membrane permeability and the concentration and hydrolysation efficiency of the periplasmic β-lactamase. When κ is small, i.e., when the hydrolysation rate is low relative to the influx of CTX, (1) implies that $C - C_p$ is also small, such that the CTX concentrations outside the cell and within the

periplasm are nearly equal. Conversely, when κ is much larger than C/K_m, then κ on the right-hand-side of (1) is by itself already larger than the left-hand-side and hence, in order for equality to hold, the factor multiplying κ must be small. This implies that the concentration C_p of CTX inside the periplasm is much lower than the outside concentration C.

For *E. coli* K12, Nikaido and collaborators have measured the permeability P, as well as the reaction constants for CTX hydrolysation by the chromosomally encoded β-lactamase AmpC, finding $P = 1.8 \cdot 10^{-5}\, cm/s$, $k_{\text{cat}} = 0.06\, s^{-1}$ and $K_m = 0.16\, \mu M$ [40, 41]. Assuming an *E. coli* volume of $1.3\, \mu m^3$, a surface area of $6.28\, \mu m^2$, and estimating the volume of the periplasm to be 30% of the cell volume [68], we find that κ depends on the number n_β of AmpC molecules per cell volume as $\kappa_{K12} = 5.5 \cdot 10^{-4}\, n_\beta$. Typical values for n_β are of the order of a few hundreds, and depend on the composition of the culture medium [45] (see also https://biocyc.org/gene?orgid=ECOLI&id=EG10040#showAll).

Nitrocefin assay of β-lactamase activity in the absence of CTX

Nitrocefin is a chromogenic cephalosporin whose hydrolysis rate can be measured to quantify the β-lactamase activity of a culture. Here, we measured β-lactamase activity of both *E. coli* strains in the absence of CTX to assess differences in per-cell AmpC expression level under the assumption that K12's and REL606's AmpC's have similar CTX hydrolysis capacity.

We made a nitrocefin solution stock by dissolving 5 mg nitrocefin in 500 μl dimethyl sulfoxide (DMSO, Sigma Aldrich) and added 9.5 ml phosphate buffer (100 mM, pH 7) to obtain a total volume of 10 ml. The stock solution was kept in a freezer at $-20°$C for a maximum of 2 months. We performed nitrocefin assays on the spent medium collected from overnight cultures of both strains to quantify the amount of β-lactamase produced by the cells in the absence of antibiotic stress. We grew eight replicate cultures for both strains (REL606 and K12) for 22 h in LB without CTX, and subsequently split each into two subpopulations. One subpopulation was subjected to sonication for 2 minutes to lyse all cells, and the medium was filtered (using a a sterile 0.2 μm syringe filter) to harvest the sonicated spent medium. The other subpopulation was centrifuged (12k RPM for 10 minutes), after which the cells were filtered out with a sterile 0.2 μm syringe filter, to obtain the not-sonicated spent medium. Then we mixed 100 μl of the spent media with 100 μl of the 10 μg/ml nitrocefin solution stock, diluting the nitrocefin solution stock concentration by a factor of 50, in a 96-well plate. The β-lactamase activity was quantified by the rate of change in the red absorption (OD490) due to nitrocefin hydrolysation (https://www.sigmaaldrich.com/deepweb/assets/sigmaaldrich/product/documents/400/065/mak221-tech-bulletin-mk.pdf and [19]).

Supplementary Table

Experiment	Figure	[CTX]
Exp 1	Fig 1 a	$0 - 0.329\,\mu$g/ml
Exp 2	Fig 1 c	$0.08\,\mu$g/ml
Exp 3	Fig 2	$0.2\,\mu$g/ml
Exp 4	Fig 3 a	$0 - 1.222$ in steps of 0.111 μg/ml
Exp 5	Fig 3 b	$0 - 0.777$ in steps of 0.111 μg/ml
Exp 6	Fig 3 c and d	$0 - 0.777$ in steps of 0.111 μg/ml
Exp 7	Fig 4 a	$0.006 - 0.113$ in steps of $0.003\,\mu$g/ml
Exp 8	Fig 4 b	$0.047 - 0.398$ in steps of $0.035\,\mu$g/ml
Exp 9	Fig 4 c	8-fold increases between 0.008 and 5.625 μg/ml
Exp 10	Fig S1 a	0.094 μg/ml
Exp 11	Fig S1 b	$0.038 - 0.206$ in steps of $0.028\,\mu$g/ml
Exp 12	Fig S2	0.08 and $0.25\,\mu$g/ml
Exp 13	Fig S3	$0 - 0.113\,\mu$g/ml
Exp 14	Fig S4	4-fold increases between 0.002 and 10 μg/ml

Table S1: The table lists the CTX concentration ranges used to obtain the experimental results presented in the corresponding figures.

Supplementary figures

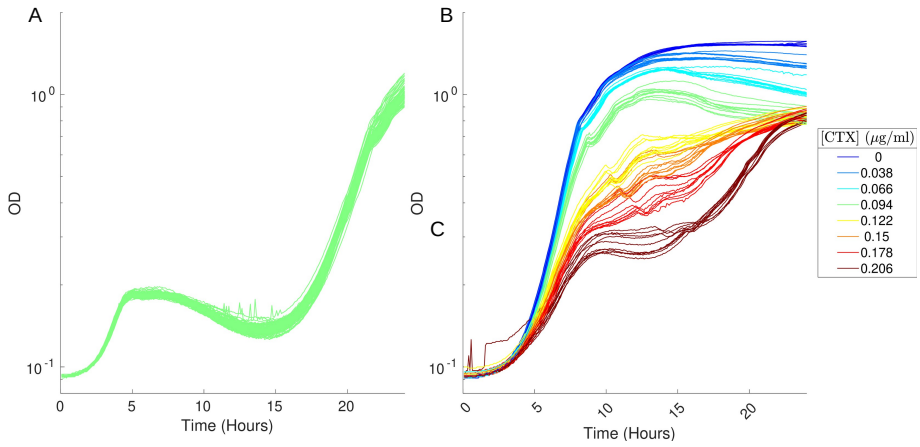

Figure S1: **Recovery growth is not due to resistance mutations.** The experiment was done in two phases. **A**: In the first phase, 80 replicate cultures of *E. coli* REL606 were grown at 0.094 μg CTX/ml for 24h. **B**: We then harvested the cells, washed them with fresh LB medium, and created 10 independent cultures by pooling eight replicate cultures for each inoculum. Dilutions from these inocula were used to start 80 new cultures in the presence of eight CTX concentrations.

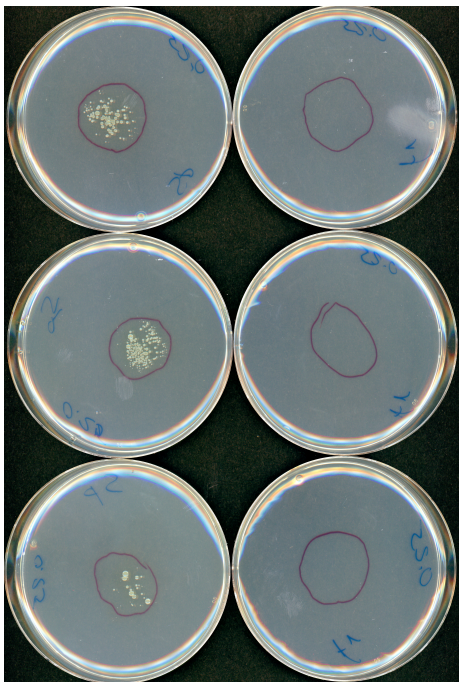

Figure S2: **Test of protection by spent medium on agar.** The figure shows six plates prepared with 20 ml LB with agar and 0.25 μg CTX/ml. In the left column, the red circles represent the area where 200 μl drops of spent medium from cultures grown for 14 h in the presence of 0.08 μg CTX/ml were placed and allowed to dry for 6 h. In the right column, the circles represent the area of control drops of fresh medium. Visible growth is detected only in the area covered by spent medium.

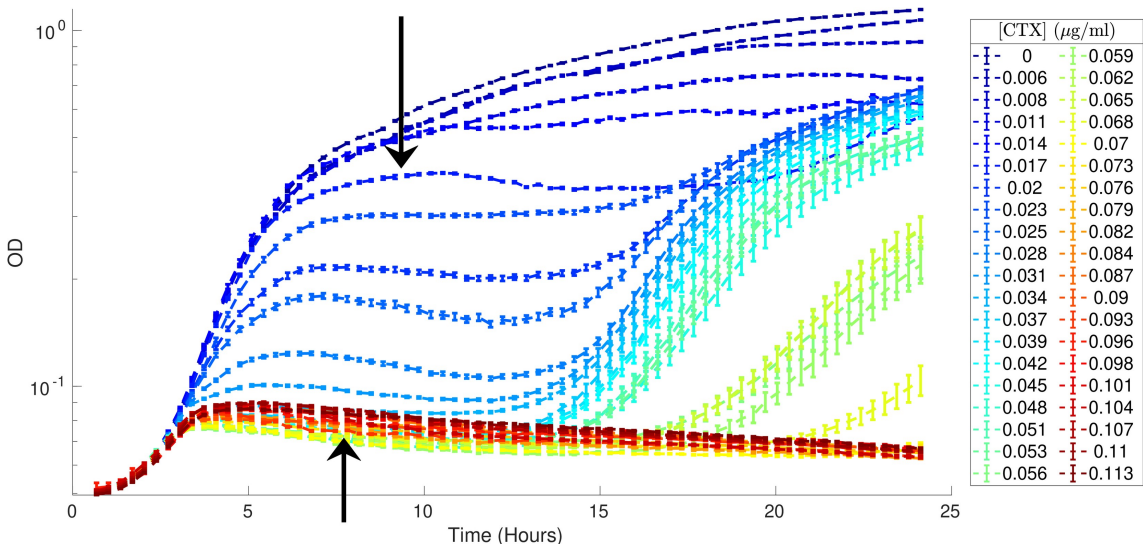

Figure S3: **Growth curves of *E. coli* K12 in a linear CTX concentration gradient.** Shown are the average and SD of OD obtained from 24 cultures of *E. coli* K12 in a linear CTX concentration gradient, ranging from $0 - 0.113\,\mu$g/ml. The inoculum size was $5 \cdot 10^5$ cells/ml (see Materials and Methods for details). For concentrations below $0.014\,\mu$g CTX/ml, the growth curves increase monotonically, saturating at late times. For concentrations above $0.014\,\mu$g CTX/ml and below $0.076\,\mu$g CTX/ml (indicated by the arrows), the growth curves exhibit non-monotonic behavior: initial growth leads to a maximum, which is followed by a decay of biomass until approximately $t = 12$ h, before growth resumes. For CTX concentrations above $0.076\,\mu$g/ml, the initial growth is followed by monotonic biomass decay.

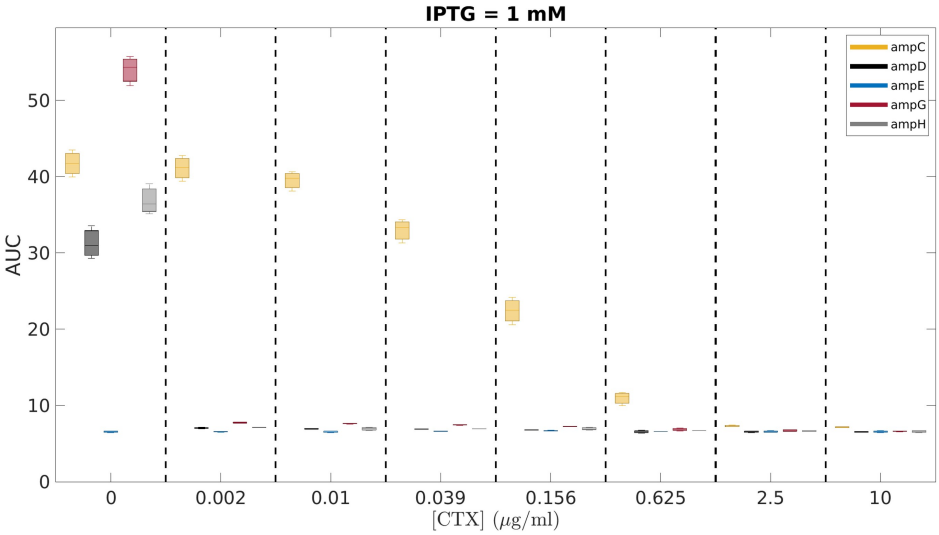

Figure S4: ***AmpC* is the only *amp* gene whose expression increases CTX resistance.** The figure shows the area under the OD-curves (AUC) of the first 30 h of growth for five different ASKA strains, in which the genes *ampC*, *ampD*, *ampE*, *ampG*, and *ampH* were overexpressed at an IPTG inducer concentration of 1 mM. Each bin corresponds to one CTX concentration.

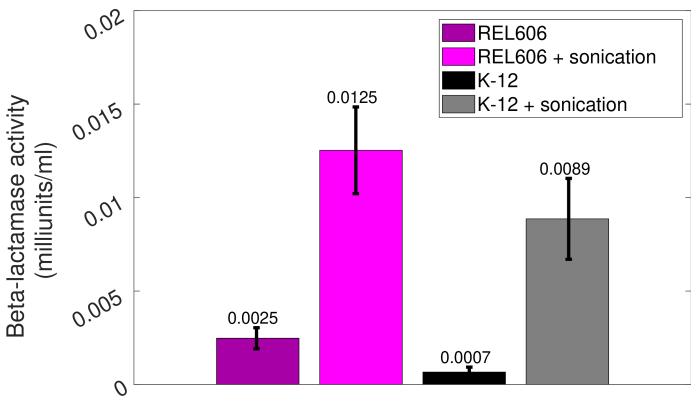

Figure S5: ***E. coli* REL606 and K12 express β-lactamase in the absence of CTX.** Eight replicates each of *E. coli* REL606 and K12 were grown for 22 h in a drug-free medium. Then each of the populations was harvested, split into two, and one of the subpopulations was subjected to sonication for two minutes to lyse the cells. Nitrocefin assays were conducted on both subpopulations in order to measure hydrolysation rates of the chromogenic cephalosporin nitrocefin by the β-lactamase present in the medium The bar plot shows the averages and SD of the 8 replicates. Both sonicated samples show a high rate of β-lactamase activity despite the fact that the cell cultures had not been subjected to antibiotic stress. All pairwise comparisons are highly significant ($P \leq 10^{-6}$ based on a Mann-Whitney U-test).

Supplementary Information: Data analysis and modeling

Feature extraction from OD curves

Figure S6 shows a typical family of 40 OD curves obtained from the growth of replicate cultures. Each OD curve represents growth under a different concentration of CTX and is color-coded from light orange to dark red, as indicated in the legend of the figure. For low concentrations of CTX, the OD growth is monotonic with saturation at late times.

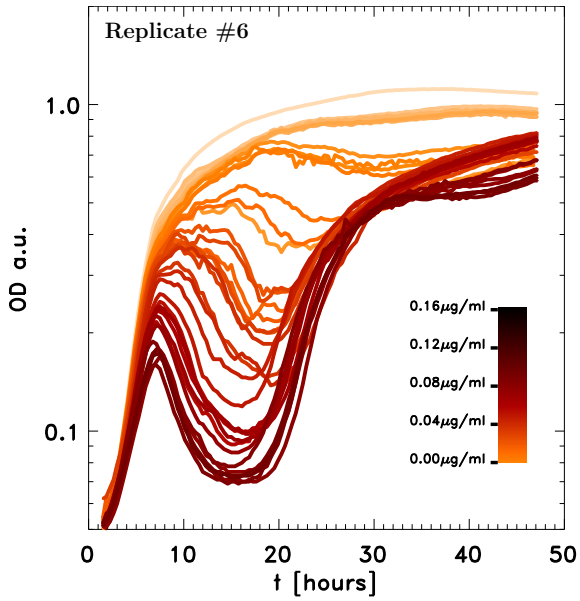

Figure S6: **Family of OD growth curves of the REL606 strain in a linear gradient of CTX concentrations, color coded as shown in the legend**. With increasing concentrations, the curves cross over from monotonic to non-monotonic growth.

We characterize the growth curves by the time t_G at which the exponential growth rate is maximum. As the CTX concentration is increased, the monotonic OD growth crosses over into non-monotonic growth. Figure S7 shows a sample non-monotonic OD curve for *E. coli* REL606 at a CTX concentration of 0.085 μg/ml. The curve exhibits a local maximum and minimum of the OD at the points labeled P and Q, respectively. These points mark three phases of population growth: an initial growth phase characterized by a maximum growth rate at point G, an intermediate decay with the decay rate becoming largest at L, and finally a recovery growth phase with maximum recovery growth attained at point R.

We implemented an automatic work flow to extract these features from the measured OD curves, determining first whether the growth is monotonic or not. If so, we identify the point G, as well as the time and corresponding exponential growth rate at G. If the growth is non-monotonic, we also determine the maximum decay – and if present – recovery growth rates, the times where these are attained, as well as the times and OD values of the local extrema, points P and Q. In the following we provide details on the extraction of these features.

We estimate instantaneous growth rates by log-fitting a moving window of n_{fit} consecutive OD data points to a straight line. Note that OD values are measured every 20 minutes. Since the initial growth rate attains its maximum in a rather short time (less than 8h after the start of the experiment), we chose $n_{\text{fit}} = 5$ data points for the window width, corresponding to a time window of 100 minutes. For the estimation of all other growth rates, we chose $n_{\text{fit}} = 12$. We defined the growth rate as the maximum of the log-fitted instantaneous rates over a time interval from $t_{\min} = 1.2h$h to $t^G_{\max} = 8h$, as indicated by the corresponding dashed vertical lines in Fig. S7.

For the determination of the intermediate decay and recovery growth rates and the local OD maxima and minima, we first check whether the OD curve is non-monotonic. We do this by testing for the existence of a local maximum of the OD. Since the OD curves, particularly around the transition from monotonic to non-monotonic growth, are noisy, we first pass the curves through a Gaussian filter in order to smoothen them. The thick curve in light grey shown in Fig. S7 is the filtered version of the measured OD curve shown in orange-red. We use the filtered OD curves to test for the existence of a local extremum. In practice, we do this by setting a maximum time

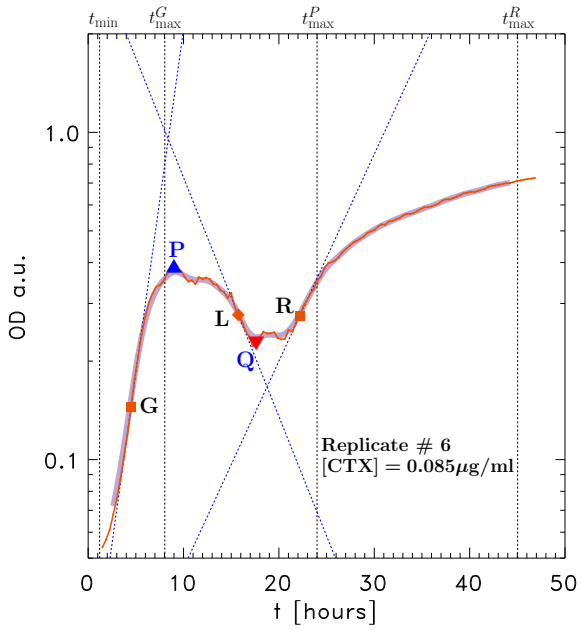

Figure S7: **A sample non-monotonic OD curve, illustrating the features of interest that we extract from it**. These are the points P and Q where the OD curve attains its local maximum and minimum, if they exist, as well as the points G, L, and Q, where the rates of initial OD growth, intermediate decay, and recovery are largest. The times $t^G_{\max}$, $t^P_{\max}$, and $t^R_{\max}$ are the cut-off times up to which we search for these features, and are indicated by the corresponding dashed vertical lines. Refer to the text for further details.

$t^P_{\max} = 24h$, such that if a local OD maximum is not found before that, we regard the OD curve as monotonically increasing. If a maximum and hence the point P was identified, we also checked whether the OD curve reaches a local minimum afterwards. If so, we identify the OD value and time t_Q where it was attained.

In the case that the OD curve is non-monotonic, we also determine the point L where the intermediate decay rate is maximum, which must be located in time after t_P. If a local minimum Q was found, we search for the maximum of the recovery growth rate in the time interval starting from t_Q up to a cut-off time $t^R_{\max}$. For the REL606 data, for which time-series were obtained up to $t = 60$h, we used an upper cut-off of $t^R_{\max} = 45h$, while for the K12 data the cut-off was $t^R_{\max} = 20$h.

The dashed blue lines in Fig. S7 indicate the fitted OD growth rates. These are the data points plotted in Fig. 1B of the main text. As noted before, for REL606 and at experimental observation times larger than $t = 45$h, the recovery of cultures subjected to high CTX concentrations shows considerable fluctuations from replicate to replicate, as evidenced by the large standard deviations in Fig. 1A. We, therefore, discarded the experimentally observed recovery rates for CTX concentrations larger than $0.250\,\mu$g/ml.

Modeling CTX hydrolysis in the periplasm and extracellular medium

Our modeling approach involves linking the enzyme production, i.e. via cell growth and its subsequent release into the extracellular medium by lysis, with the known kinetics of CTX hydrolysis by β-lactamases. Similar modeling approaches have been put forward before. Andreani and collaborators have considered hydrolysis due to cell lysis and subsequent release of β-lactamases into the extracellular medium [42, 34]. They assume that lysis starts to occur once the filamented cell length exceeds a CTX concentration dependent critical length. This length marks the onset where the rate at which damage to the peptidoglycan layer due to CTX exceeds the rate at which the cell can repair the damage. Artemova and collaborators analysed a model where CTX is hydrolysed both inside the periplasm and in the extracellular medium. Lysis is assumed to occur once the CTX concentration inside the periplasm exceeds a threshold value, which they call the single cell MIC [12]. Recently, Geyrhofer and collaborators have considered a model that does not explicitly take lysis into account, but assumes that there is an outflux of β-lactamase into the extracellular medium from intact cells [18].

Our modeling strategy follows that of Artemova et al. [12], but in addition we estimate the production rates of viable and lysed biomass from the empirical OD curves that we obtained at

various CTX concentrations. We use these rates as inputs to our modeling of the chemical kinetics of CTX hydrolysis by β-lactamases. We further assume that the β-lactamases are confined to the periplasm where they can diffuse freely, unless the cells lyse [46]. In our model, hydrolysis of CTX by β-lactamase can therefore take place either inside the periplasm of non-lysed cells or in the extracellular medium, in which case the amount of β-lactamases available at any given time will depend on the biomass that has lysed so far. We ignore processes that lead to a natural degradation of CTX or β-lactamases, assuming that the corresponding decay times are much larger than the duration of our experiments.

The diffusion of β-lactams across the outermembrane bilayer is negligible and their entry into the periplasm occurs through the porins [66, 66, 67]. The influx of CTX via porins into the periplasm is assumed to be governed by Fick's law

$$\mathcal{V}_{\text{peri}} \frac{\mathrm{d}C_p}{\mathrm{d}t} = PA(C_0 - C_p), \tag{4}$$

where P is the permeability constant, A is the *E. coli* surface area, $\mathcal{V}_{\text{peri}}$ is the periplasmic volume, and C_0 and C_p are the CTX concentration outside the cell and inside the periplasm, respectively.

The hydrolysis of CTX via β-lactamases in the periplasm follows a Michaelis-Menten type kinetics:

$$\frac{\mathrm{d}C_p}{\mathrm{d}t} = -k_{\text{cat}} E \frac{C_p}{K_m + C_p}, \tag{5}$$

where E is the concentration of β-lactamase, while k_{cat} and K_m are the rate constants of the CTX hydrolysis reaction kinetics.

An equilibrium is established once the concentration of CTX inside the periplasm is constant in time, implying that the influx rate of CTX via porins is balanced by the hydrolysis rate inside the periplasm, leading to the Zimmermann-Rosselet Equation [44]

$$C_0 = C_p + k_{\text{cat}} \frac{\mathcal{V}_{\text{peri}}}{PA} E \frac{C_p}{K_m + C_p}. \tag{6}$$

It is convenient to go to units in which the concentrations are measured relative to K_m. Thus defining $a_0 = C_0/K_m$ and $a_p = C_p/K_m$ the influx and hydrolysis equations are given by

$$\frac{\mathrm{d}a_p}{\mathrm{d}t} = \frac{PA}{\mathcal{V}_{\text{peri}}}(a_0 - a_p), \tag{7}$$

$$\frac{\mathrm{d}a_p}{\mathrm{d}t} = -\frac{k_{\text{cat}}}{K_m} E \frac{a_p}{1 + a_p}. \tag{8}$$

Thus (6) becomes

$$a_0 - a_p = \kappa \frac{a_p}{1 + a_p}, \tag{9}$$

where we have introduced the dimensionless quantity

$$\kappa = \frac{k_{\text{cat}}}{K_m} \frac{\mathcal{V}_{\text{peri}}}{PA} E, \tag{10}$$

which essentially is the ratio of the rate of CTX hydrolysis to the influx rate.

It is clear that the CTX gradient $a_0 - a_p$ across the outermembrane depends on the value of κ. If $\kappa \ll 1$, then the hydrolysis rate is small compared to the influx rate and from (9) we see that $a_0 - a_p$ is of the order of κ. Hence the difference of CTX concentrations outside and inside the periplasm is small. Conversely, if $\kappa \gg a_0$, then the hydrolysis rate is relatively high, meaning that any CTX molecule that diffuses into the periplasm is rapidly hydrolysed so that large concentration differences can be maintained. Indeed we find that in this limit, a_0/a_p is of order κ.

Another point worth stressing is that for the values quoted in the main text, it follows from (7) and (8) that the equilibration of the CTX concentration inside the periplasm is very rapid and reached within seconds [40]. Since in typical settings, such as our experiments, the CTX is hydrolysed over a time scale of hours, this means that the CTX concentration inside the periplasm is in quasistatic equilibrium throughout, i.e we can assume that (9) holds although a_p and a_0 change (sufficiently slowly) in time. We will refer to this as the quasistatic approximation.

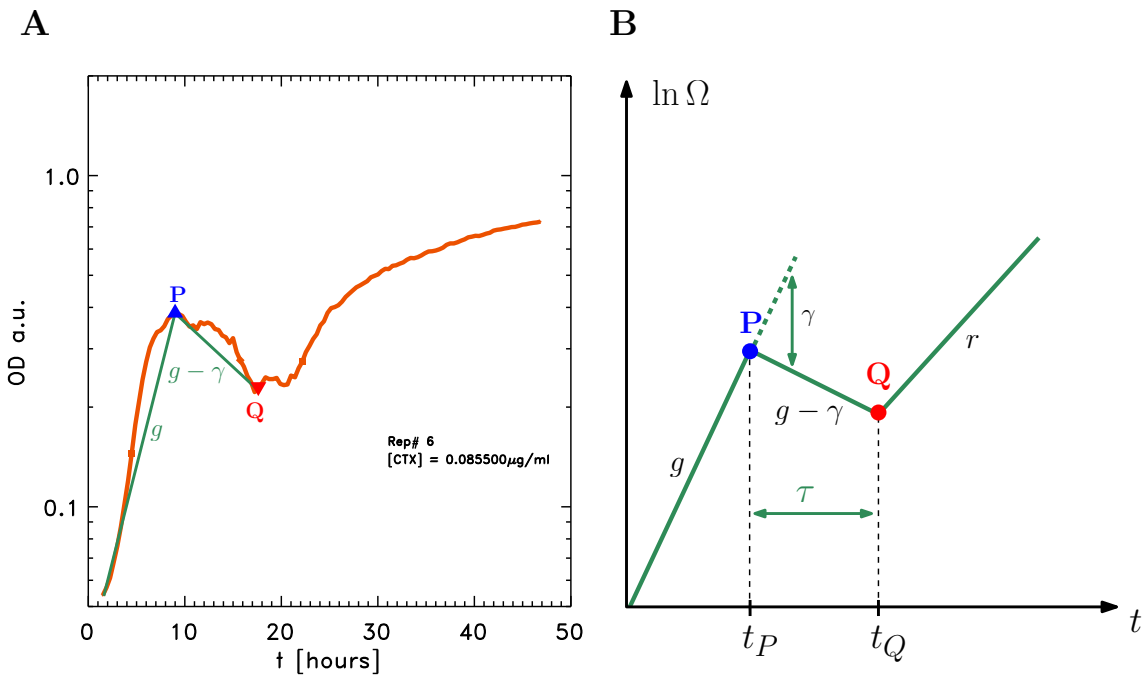

Figure S8: **Modeling *E. coli* growth. A**: Experimentally obtained OD curve for *E. coli* strain REL606 at a CTX concentration of 0.0855 μg/ml. The OD reaches a peak OD_P at time t_P that is followed by a decay and subsequent onset of recovery at t_Q and OD_Q. The green lines represent an average constant initial growth and intermediate decay rate, as inferred from the OD curve. **B**: The simplified growth curve used in our modeling. We assume initial growth of biomass at fixed exponential growth rate g, which is followed at time t_P by simultaneous decay due to lysis and continuing growth, given by the effective rate $m = g - \gamma$. Here γ is the rate of cell lysis. At point Q exponential growth resumes again with some growth rate r. The recovery time $\tau = t_Q - t_P$ is defined to be the time between the onset of lysis and the beginning of recovery.

Coupling CTX hydrolyzation to *E. coli* growth and eventual lysis

We are interested in modeling the non-monotonic growth and recovery of the population at intermediate CTX concentrations. Figure S8A shows the typical OD behavior. Initially, the OD grows, reaching local maximum OD_P at point P and time t_P. This point marks the onset of OD decay continuing up to point Q, which is reached at time t_Q and OD_Q. For times larger than t_Q, the OD starts to grow again, which marks the onset of recovery of the bacterial population. Panel B is a simplified picture of this OD behavior, expressed now in terms of the biomass Ω. We assume that up to time t_P the biomass growth is exponential with fixed growth rate g, while between P and Q we assume that the biomass is decaying at a rate $m = g - \gamma$, where γ is the cell lysis rate, assumed to be constant in time. Beyond Q, the biomass resumes exponential growth with rate r.

In the present section, we will assume that the growth of biomass, as shown in Fig. S8B, is given as input into our modeling and specified in terms of the biomass Ω_P at P and time t_P, as well as the *mean* initial growth and intermediate decay rates g and m. For the given range of CTX concentrations, we can estimate these parameters from the measured OD curves, as indicated by the green lines in panel A of Fig. S8. Assuming that recovery sets in once the CTX concentration in the medium has fallen due to hydrolysis below a certain concentration, our goal is to work out the time when this occurs, i.e. the recovery time $\tau = t_Q - t_P$.

Let us emphasize that we assume that the growth and subsequent lysis rates are constant in time, but that their overall values can depend on the antibiotic concentration. However, the antibiotic concentration in turn does depend on time, due to the hydrolysis. In our modeling, we will consider this time dependence of growth rates as a second order effect, which we take care of by assuming that g and γ denote effective or mean growth and lysis rates, that thereby take into account in part an implicit time-dependence due to the change of concentrations. Practically, this is conveniently achieved by approximating the curved pieces of the log OD curve by linear segments, which leads to the piece-wise linear growth of log-biomass as shown in Fig. S8A and B. Following Geyrhofer et al. [18], it is possible to incorporate an explicit dependence of growth and lysis rates on instantaneous antibiotic concentration. While such a modeling is more realistic

and will also round out the biomass growth at points P and Q, it comes at the price of analytical complexity. Since our main aim of modeling is to obtain a qualitative as well as rough order of magnitude quantitative understanding, we prefer to work with effective and constant exponential growth and decay rates.

For the range of CTX concentrations that give rise to non-monotonic OD growth, we assume that in the initial growth state cells filament, but do not lyse, so that cell length grows as

$$\ell(t) = \ell_0 e^{gt}, \tag{11}$$

where ℓ_0 is the length of a cell of normal size. Assuming an inoculum size of N_0 cells, the (linear) biomass grows as

$$\Omega(t) = N_0 \ell_0 e^{gt} = \Omega_0 e^{gt}. \tag{12}$$

up to time $t = t_P$. At P, cells start to lyse at a constant rate γ. Thus for $t > t_P$, cells continue growing at exponential rate g, while some of them lyse at rate γ and we find

$$\Omega(t) = \Omega_P \, e^{-(\gamma - g)(t - t_P)}. \tag{13}$$

We first work out the reaction kinetics of CTX hydrolyzation outside the cells, i.e. in the extracellular medium. This process is driven by the release of β-lactamase molecules into the extracellular medium by lysis, leading to a gradual rise of the enzyme concentration. Let $E_{\mathrm{ly}}(t)$ be the concentration of β-lactamase in the extracellular medium so that $E_{\mathrm{ly}}(t) = 0$ for $t \leq t_P$ (no lysis yet). For $t > t_P$, we assume that the break-down of CTX is by hydrolysis and follows the Michaelis-Menten type reaction kinetics discussed before,

$$\frac{\mathrm{d}a}{\mathrm{d}t} = -\frac{k_{\mathrm{cat}}}{K_m} E_{\mathrm{ly}} \frac{a}{1+a}, \tag{14}$$

where $a = C/K_m$ is the dimensionless CTX concentration C in units of K_m. The amount of $E_{\mathrm{ly}}(t)$ accumulates as a result of the lysis of cells and hence is given by

$$\frac{\mathrm{d}E_{\mathrm{ly}}}{\mathrm{d}t} = \rho\gamma \frac{\Omega}{\mathcal{V}}, \tag{15}$$

where $\gamma\Omega$ is the amount of biomass lysed per unit time, $\mathcal{V}$ is the volume of the container, and ρ is the number of β-lactamase molecules contained per biomass. Since the time evolution of Ω is known, and setting $\tau = t - t_P$, we have

$$E_{\mathrm{ly}}(\tau) = \frac{\gamma}{\gamma - g} E_P \left(1 - e^{-(\gamma - g)\tau}\right). \tag{16}$$

Here, E_P is the effective concentration of β-lactamase in the extra cellular medium that would have been attained if all the cells present at P had lysed at once. Substituting (16) into (14), we find that the rate at which CTX is hydrolysed in the extracellular medium is given by

$$\left(\frac{\mathrm{d}a}{\mathrm{d}\tau}\right)_{\mathrm{medium}} = -\frac{k_{\mathrm{cat}}}{K_m} \frac{\gamma}{\gamma - g} E_P \left(1 - e^{-(\gamma - g)\tau}\right) \frac{a}{1+a}. \tag{17}$$

Let us now turn to the hydrolysis of CTX inside the periplasm. Denoting by E_{cell} the concentration of β-lactamase in the periplasm and recalling that we are in the quasistatic regime, we have, cf. (9),

$$a - a_p = k_{\mathrm{cat}} \frac{V_{\mathrm{peri}}}{PA} \frac{E_{\mathrm{cell}}}{K_m} \frac{a_p}{1+a_p} \equiv \kappa \frac{a_p}{1+a_p}. \tag{18}$$

For *E. coli* K12 and the concentrations of interest $\kappa \sim 0.39$ (see main text), and we therefore assume that κ is small. Then, replacing a_p by a on the right hand side of (18) introduces an error of order κ which we will neglect, and we thus make the approximation

$$a - a_p = \kappa \frac{a}{1+a}. \tag{19}$$

The total flow rate of CTX into the cells by diffusion is given by

$$\left(\frac{\mathrm{d}a}{\mathrm{d}\tau}\right)_{\mathrm{peri}} = -\nu \frac{\ell_{\mathrm{fil}}}{\ell_0} PA(a - a_p), \tag{20}$$

where ν is the concentration of cells, i.e. number of (filamented) cells per unit volume, while A and $A\ell_{\mathrm{fil}}/\ell_0$ are the surface area of normal-sized and filamented cells, respectively. Here ℓ_{fil} is the

length of filamented cells at time τ, cf. (11). At equilibrium, (20) furnishes also the rate at which the CTX is hydrolysed inside the periplasm, so that this can be written as

$$\begin{aligned}\left(\frac{\mathrm{d}a}{\mathrm{d}\tau}\right)_{\mathrm{peri}} &= -\nu\,\frac{\ell_{\mathrm{fil}}}{\ell_0}E_{\mathrm{cell}}V_{\mathrm{peri}}\,\frac{k_{\mathrm{cat}}}{K_m}\frac{a}{1+a}\\ &= -\nu\,\frac{\ell_{\mathrm{fil}}}{\ell_0}n_\beta\frac{k_{\mathrm{cat}}}{K_m}\frac{a}{1+a}\\ &= -E_P e^{-(\gamma-g)\tau}\,\frac{k_{\mathrm{cat}}}{K_m}\frac{a}{1+a}.\end{aligned} \tag{21}$$

Note that since V_{peri} is the periplasmic volume of a cell of normal size, $E_{\mathrm{cell}}V_{\mathrm{peri}} = n_\beta$ is the number of β-lactamase molecules in a normal-sized cell while multiplying this with $\ell_{\mathrm{fil}}/\ell_0$ yields the total number of β-lactamase molecules in the periplasm of all filamented cells with average filament size ℓ_{fil}. Combining this with the concentration ν of filamented cells, yields the expression in the last line of (21), where E_P is again the concentration of β-lactamase in the medium if at P all cells had lysed simultaneously.

We have thus worked out the contributions to the reduction of CTX concentration in the extracellular medium due to hydrolysis outside and inside the periplasm, as given by (17) and (21). Combining both equations gives

$$\frac{\mathrm{d}a}{\mathrm{d}\tau} = -\frac{E_P}{K_m}\frac{k_{\mathrm{cat}}}{\gamma-g}\left(\gamma - g\,e^{-(\gamma-g)\tau}\right)\frac{a}{1+a}, \tag{22}$$

describing the evolution of the CTX concentration in the medium at times $\tau = t - t_P$ since the onset of lysis at point P.

What remains to be done is the estimation of the CTX concentration at $\tau = 0$, i.e. $t = t_P$. This concentration is less than the initial CTX concentration, since during times up to t_P some CTX has already been hydrolysed in the periplasm. As we neglect lysis during the initial growth phase and further assume a constant number of enzyme molecules per unit biomass, we find that for $0 \le t \le t_P$, the CTX concentration of the medium changes as

$$\frac{\mathrm{d}a}{\mathrm{d}t} = -E_0 e^{gt}\,\frac{k_{\mathrm{cat}}}{K_m}\frac{a}{1+a}, \tag{23}$$

or if we are extrapolating from t_P, so that $E_P = E_0 e^{gt_P}$,

$$\frac{\mathrm{d}a}{\mathrm{d}t} = -E_P e^{-g(t_P-t)}\,\frac{k_{\mathrm{cat}}}{K_m}\frac{a}{1+a}. \tag{24}$$

The solution of (24) can be found by direct integration and leads to the implicit form

$$a_P + \ln a_P = a_0 + \ln a_0 - \frac{E_P}{K_m}\frac{k_{\mathrm{cat}}}{g}\left(1 - e^{-gt_P}\right), \tag{25}$$

where a_0 is the initial CTX concentration of the culture, while a_P is the concentration at time t_P, corresponding to onset of lysis. Similarly for $\tau = t - t_P > 0$, the solution of (22) is given by

$$a_\tau + \ln a_\tau = a_P + \ln a_P - \frac{E_P}{K_m}\frac{k_{\mathrm{cat}}}{\gamma-g}\left[\gamma\tau - \frac{g}{\gamma-g}\left(1 - e^{-(\gamma-g)\tau}\right)\right]. \tag{26}$$

Combining (25) with (26) we thus obtain the evolution of the CTX concentration at times τ after the onset of lysis in terms of the reaction constants of the hydrolysis k_{cat} and K_m, the concentration E_P of β-lactamase molecules at time t_P, the initial CTX concentration a_0, as well as the initial growth rate g and the lysis rate γ. Exponentiating both sides of these equations, we see that a_τ is given in terms of Lambert functions, i.e. solutions to equations of the form $a_\tau \exp(a_\tau) = C$, which can be obtained numerically. The initial concentration of CTX is known, and for *E. coli* K12 we estimated the cross-over from monotonic growth to non-monotonic growth as $[\mathrm{CTX}] = 0.015\,\mu\mathrm{g/ml}$ so that the final CTX concentration a_τ, marking the onset of recovery is known as well. The only adjustable parameter is E_P, or equivalently the number n_β of β-lactamase molecules per volume of a normal-size cell. Given n_β, E_P is then inferred from the inoculum size of $5 \cdot 10^5$ cells per ml, and the experimentally obtained values for t_P and the initial growth rate g. For our *E. coli* K12 data, the choices of $n_\beta = 500, 700$ and 900 lead to the three predictions of τ shown in Fig. 5A.

Finally, let us also work out the case when the *E. coli* strain is such that $\kappa \gg a$. As we argued in the main text, we expect this to resemble *E. coli* REL606 more closely. In this case, we approximate the solution of (9) as

$$a - a_p = \kappa a_p, \tag{27}$$

by neglecting the denominator on the RHS of that equation, since the choice of $\kappa \gg \max(a, 1)$ implies that a_p is of order $1/\kappa$ and hence small, so that

$$a_p = \frac{a}{\kappa + 1} \approx \frac{a}{\kappa}. \tag{28}$$

As before, the hydrolysis of CTX in the extracellular medium is given by (17) and does not change. The reduction of CTX due to hydrolysis inside the periplasm is driven by the concentration gradient (20), and hence depends on a_p. Substituting (28) into (20), we find that

$$\left(\frac{\mathrm{d}a}{\mathrm{d}t}\right)_{\mathrm{peri}} = -e^{-(\gamma-g)\tau} \left[\frac{k_{\mathrm{cat}}}{\kappa}\right] \frac{E_P}{K_m}\, a. \tag{29}$$

We can think of the term in rectangular brackets as an effective hydrolyzation rate that is modulated by κ. Comparing (21) with (29), we see that the overall rate of CTX hydrolysis inside the periplasm is reduced by the additional factor of $1/\kappa$.

Let us therefore assume that hydrolysis inside the periplasm is negligible. Then the CTX is hydrolyzed only in the extracellular medium and this implies in particular that up to $t = t_P$ hydrolysis is negligible and hence $a_0 = a_P$. From (17) we thus find that

$$a_\tau + \ln a_\tau = a_0 + \ln a_0 - \frac{E_P}{K_m}\, k_{\mathrm{cat}}\tau\, \frac{\gamma}{\gamma - g} \left(1 - \frac{1 - e^{-(\gamma-g)\tau}}{(\gamma - g)\tau}\right). \tag{30}$$

For *E. coli* REL606, we estimated the cross-over concentration from monotonic to non-monotonic OD growth as $[\mathrm{CTX}] = 0.06\,\mu\mathrm{g/ml}$, so that a_τ is known and the only adjustable parameter is the number n_β of β-lactamase molecules per normal-size cell, which in turn determines E_P. For *E. coli* REL606, the choices of $n_\beta = 600, 1000$ and 1400 lead to the three predictions for τ shown in Fig. 5B.